

# Reconstructing basal ice flow patterns of the Last Glacial Maximum Rhine glacier (northern Alpine foreland) based on streamlined subglacial landforms

Sarah Kamleitner<sup>1</sup>  | Susan Ivy-Ochs<sup>1</sup>  | Bernhard Salcher<sup>2</sup>  |  
Jürgen M. Reitner<sup>3</sup> 

<sup>1</sup>Laboratory of Ion Beam Physics, ETH Zürich, Zürich, Switzerland

<sup>2</sup>Department of Geography and Geology, Paris Lodron University of Salzburg, Salzburg, Austria

<sup>3</sup>Department of Geological Mapping, GeoSphere Austria, Vienna, Austria

## Correspondence

Sarah Kamleitner, Laboratory of Ion Beam Physics, ETH Zürich, Zürich, Switzerland.  
Email: [kamsarah@phys.ethz.ch](mailto:kamsarah@phys.ethz.ch)

## Funding information

Schweizerischer Nationalfonds zur Förderung der Wissenschaftlichen Forschung, Grant/Award Number: 175794, 2017

## Abstract

Based on high-resolution (sub)glacial geomorphological mapping, we present a first digital inventory of streamlined bedforms within the footprint of a Last Glacial Maximum (LGM) Alpine piedmont glacier. A total of 2460 drumlins were mapped across the Rhine glacier foreland. Glacial lineations and one field of subglacial ribs (ribbed/Rogen moraines) – the first record of this type of subglacial landform on the Alpine foreland—were identified. Two flowsets, associated with (i) the Rhine glacier's LGM maximum advance (Schaffhausen stadial) and (ii) a late LGM readvance (Stein am Rhein stadial), are differentiated. The vast majority of streamlined bedforms occur in fields aligned in a 16- to 30-km-wide swath upstream of the Stein am Rhein frontal moraines. Orientation and elongation of drumlins and glacial lineations set the basis for the reconstruction of paleo-ice flow. Basal flow paths of the LGM maximum advance are visually interpreted and restricted to the zone proximal to the former ice front. The flow field reconstructed for the late LGM glacier readvance (Stein am Rhein stadial) extends tens of kilometres upstream and is modelled implementing a recently published kriging routine. The derived basal flow patterns paired with information on ice surface levels from lateral and frontal moraines and combined with relative ice velocity differences inferred from spatial changes in bedform elongation reveal detailed insights on ice flow geometries, particularly during the glacier readvance. Reconstructed flowlines highlight basal flow under shallow ice that is strongly controlled by local topography evidenced by diverging around basal bumps and converging in (narrow) valley sections and troughs, where basal flow velocities, steered by topography, are high. Gained paleo-ice basal flow patterns offer new insights on landscape evolution of the northern Alpine foreland and provide evidence-based flow data to validate future physical modelling results.

## KEYWORDS

drumlin, European Alps, glacial reconstruction, ice flow trajectories, subglacial ribs, subglacial streamlined bedforms

## 1 | INTRODUCTION

Subglacial bedforms develop at the base of wet-based glaciers when flowing ice streamlines underlying sediments or bedrock

(Boulton, 1987; Eyles et al., 2016; Menzies, 1979; Patterson & Hooke, 1995; Stokes, Spagnolo, et al., 2013) and leaves behind landforms oriented either parallel or transverse to flow (Clark, 1999; Clark, Ely, Spagnolo, et al., 2018; Stokes et al., 2011). Subglacially

This is an open access article under the terms of the [Creative Commons Attribution](https://creativecommons.org/licenses/by/4.0/) License, which permits use, distribution and reproduction in any medium, provided the original work is properly cited.

© 2023 The Authors. *Earth Surface Processes and Landforms* published by John Wiley & Sons Ltd.

streamlined landforms are widespread features in regions formerly covered by the large Northern Hemisphere ice sheets (e.g., the British and Irish [Clark, Ely, Greenwood, et al., 2018; Greenwood & Clark, 2008; Hughes et al., 2010], Scandinavian [Boyes et al., 2021; Hättestrand et al., 1999; Putkinen et al., 2017] or Laurentide ice sheets [Boulton & Clark, 1990a, 1990b; Clark, 1993; Clark et al., 2000; McMartin et al., 2021; Prest et al., 1968; Stokes, Spagnolo, et al., 2013]), and are also known from the forelands of the European Alps (Habbe, 1989, 1992). Drumlins, mega-scale glacial lineations (MSGs), flutes and subglacial ribs (also known as Rogen moraines or ribbed moraines) are typical landforms of the ice-bed interface (Clark, 2010). The process of formation of subglacial landforms, especially drumlins, is not fully understood and is discussed widely (Boulton, 1987; Clark et al., 2003; Dunlop et al., 2008; Eyles et al., 2016; Fowler & Chapwanya, 2014; Hart et al., 2018; Iverson et al., 2017; Menzies, 1979; Shaw, 2002; Stokes, Fowler, et al., 2013). As expressed succinctly by Eyles et al. (2016), one needs to envision that drumlins either emerge (are depositional) or grow down and thus are erosional landforms. But equifinality of subglacial shapes may also play a role, with different processes occurring at the ice-bed interface individually or in concert at different times (Fowler, 2018; Möller & Dowling, 2018).

Orientations of streamlined subglacial landforms indicate glacier flow directions and are a powerful tool for constraining basal ice flow patterns during past glaciations (Clark, 1999; Greenwood & Clark, 2009; Hughes et al., 2014; Kleman & Borgström, 1996; Ng & Hughes, 2019; Shaw et al., 2010; Stokes & Clark, 2001). Highly elongated subglacial features can further inform about corridors of fast-flowing ice (Jamieson et al., 2016; Stokes & Clark, 2002). Recent modelling results find a wet subglacial environment, equal to those observed under modern ice streams, to be a key requisite for drumlins elongating into MSGs (Ely et al., 2023). When basal sliding occurs under wet-based conditions, the glacier bed is continuously remodelled and subglacial landforms are formed, reshaped and destroyed, depending on ice velocity and occupation time (Clark, 1993, 1994; Kleman et al., 2007; Kleman & Borgström, 1996). Setting in of cold-based conditions, glacier-bed decoupling or de-glaciation, can lead to fossilization of streamlined bedforms (Kleman & Borgström, 1996). If wet-based conditions are reinstated and streamlining resumes, large glacial lineations of previous flow regime(s) may be preserved as patches of beheaded, cross-cut or overprinted forms (Clark, 1999; Kleman et al., 2007; Kleman & Borgström, 1996).

In the European Alps, drumlin fields are known from the former beds of the large Quaternary (piedmont) glaciers that flowed out of the high mountain areas onto the forelands (e.g., Lyon, Rhone, Reuss, Rhine, Iller, Isar-Loisach, Inn and Salzach glaciers) (Beckenbach et al., 2014; Custer & Aubert, 1935; Ebers, 1926; Früh, 1904; Glückert, 1974; Habbe, 1988; Penck & Brückner, 1909; Salcher et al., 2010; Weinberger, 1952), as well as in inner Alpine valleys (Bodenburg Hellmund, 1909; Götzinger, 1939; Heinisch et al., 2015; Schuster et al., 2006; van der Meer, 1982; van Husen, 1977). The most pronounced subglacial landforms are found internal to the Last Glacial Maximum (LGM) terminal moraines (Ivy-Ochs et al., 2022), but downstream of the LGM ice margins, drumlins formed during a larger pre-LGM glaciation exist as well (Ellwanger, 1994).

Studies on Alpine foreland drumlins date back to the late 19th and early 20th centuries. Past research focused on sedimentological composition of drumlins as well as drumlin distribution and morphology (Bodenburg Hellmund, 1909; Brückner, 1886; de Jong, 1983; Ebers, 1926, 1960; Ellwanger, 1990, 1994; Früh, 1904; German, 1977; Glückert, 1974; Grünvogel, 1953; Habbe, 1988, 1989, 1992; Schreiner, 1976). Alpine drumlins contain a range of unconsolidated sediments (till, gravel, gravel mantled by or interbedded with till, deltaic sediment and ice marginal sediment) and also can be cored by Molasse bedrock (Brauhaus, 1976; de Jong, 1983; Ellwanger, 1990, 1992; Erb, 1986; Grünvogel, 1953; Habicht et al., 1986; Saxer, 1965; Schmidle, 1914, 1916; Schmidt & Müntz, 1979; Schreiner, 1976; Zaugg & Geyer, 2008). Geomorphological maps of single drumlin fields have been published (Früh, 1904; Grünvogel, 1954; Habbe, 1989), and geological map sheets partially delineate drumlins. Nevertheless, a systematic approach to capture the subglacial record on the piedmont lobe scale is missing. Grünvogel (1954) assessed regional ice flow pattern in the eastern part of the LGM Rhine glacier based on streamlined landforms, but overall, paleo-flow information preserved in streamlined bedforms has not been made use of on the Alpine foreland.

In recent years, subglacial features on the Alpine foreland have been discussed as part of glacier dynamics (e.g., in the Salzach glacier system [Salcher et al., 2010]), but interest in Alpine drumlins seems to have waned. This is somewhat surprising as over that same time frame, the development of geographical information system (GIS) and remote sensing technologies and products (e.g., digital elevation models [DEMs] and aerial images) (Beckenbach et al., 2014; Chandler et al., 2018; Napieralski et al., 2007; Smith et al., 2006; Smith & Clark, 2005; Wagner, 2017) provided increasing opportunities to capture subglacial bedforms in their sharpness and frequency, allowing to overcome spatial limitations and to analyse glacier flow dynamics on a larger scale.

Unlocking the potential of high-resolution elevation data, we mapped in detail glacial and subglacial landforms within the former extent of the LGM Rhine glacier piedmont lobe, one of the major glacier systems of the Alps. Knowledge on the types of bedforms present and their location in the landscape can be combined with information on landform elongation and orientation to reconstruct flow conditions of paleoglaciers. Based on our mapping of over 2500 subglacial streamlined bedforms and calculated morphometric parameters, we provide an overview on type and size range of subglacial landforms on the Alpine foreland. After defining flowsets, subglacial landform orientation is used to infer the basal flow fields of paleo-Rhine glacier visually. Implementing the kriging approach of Ng and Hughes (2019), we fully reconstruct the basal flow pattern of the Rhine glacier during a late LGM readvance phase. We thereby add a new dimension of information to an in other aspects well-studied glacier system (cf. Ellwanger et al., 2011; Kamleitner et al., 2023; Keller & Krayss, 2005; Preusser et al., 2007; and references therein). The transition at the Alpine margin from strongly topographically controlled ice flow to comparatively unconstrained flow conditions in the foreland makes the Alps an exceptional test site for studying subglacial landform formation. Our reconstructed basal flow patterns further provide evidence-based flow directions to ground truth and complement numerical modelling studies

(Benz-Meier, 2003; Cohen, 2017; Cohen et al., 2018; Imhof et al., 2019; Seguinot et al., 2018).

## 2 | SETTING

The footprint of the LGM Rhine glacier piedmont lobe is located in the region of Lake Constance at the northern fringe of the European Alps. Lake Constance (396 m a.s.l.) is one of the largest peri-Alpine lakes. Its basin is located in the centre of the former ~6000-km<sup>2</sup>-sized LGM piedmont lobe of the Rhine glacier (Figure 1) (Bini et al., 2009; Ellwanger et al., 2011; Jäckli, 1962; Keller & Krayss, 2005; van Husen, 1987). On the foreland, the LGM Rhine glacier organized into four main lobes (clockwise from west to east): Thur, Untersee, Schussen and Argen lobes. Two remarkably distinct bands of frontal moraines are present (Ellwanger et al., 2011; Penck & Brückner, 1909). These demarcate the Schaffhausen (~26–22 ka; Kamleitner et al., 2023; Preusser et al., 2007) and the Stein am Rhein stadial (after ~21 ka; Kamleitner et al., 2023) extents of the LGM Rhine glacier and relate to the LGM maximum advance and a following late LGM readvance, respectively (Ellwanger et al., 2011; Kamleitner et al., 2023; Keller & Krayss, 2005; Penck & Brückner, 1909; Preusser et al., 2007; Schreiner, 1992a). Stein am Rhein glacial tills, at several sites, overlie lake and outwash deposits, highlighting the readvance character of the Stein am Rhein stadial

(Ellwanger et al., 2011; Heinz, 2001; Keller & Krayss, 2005; Schreiner, 1992b; Schindler et al., 1978). The Stein am Rhein moraines are located 5–13 km upstream of the outer Schaffhausen frontal moraines. Further inboard, moraines of a retreat stadial, the Konstanz stadial, have been mapped by some authors (Keller & Krayss, 2005; Schmidle, 1914, 1916) (see also Section 4.2).

Bedrock in the area is predominantly Molasse (Ellwanger et al., 2011; Keller, 2021; Regierungspräsidium Freiburg Landesamt für Geologie, Rohstoffe und Bergbau, 2013). Only in the very northern and northwestern regions do Jurassic limestones and Miocene volcanic rocks crop out (Hofmann, 1997; Hübscher, 1961; Regierungspräsidium Freiburg Landesamt für Geologie, Rohstoffe und Bergbau, 2013; Schreiner, 1992b). Multiple, partly overdeepened, basins and troughs were carved into the Molasse by glacial and fluvial processes over hundreds of thousands of years (Ellwanger et al., 2011; Heuberger et al., 2012; Jordan, 2010; Pietsch & Jordan, 2014; Schlunegger & Mosar, 2011; Schnellmann et al., 2014). These are typically filled with subglacial tills and deltaic, glaciofluvial and/or glaciolacustrine sediments (Buechi et al., 2017; Fiebig et al., 2011; Preusser et al., 2010; Schreiner, 1968). The Molasse bedrock is, particularly in the western and central parts of the study area, largely segregated into isolated highs that are partly covered with older Quaternary sediments (Ellwanger et al., 2011; Keller, 2021; Regierungspräsidium Freiburg Landesamt für Geologie, 2013; Schreiner, 1979).

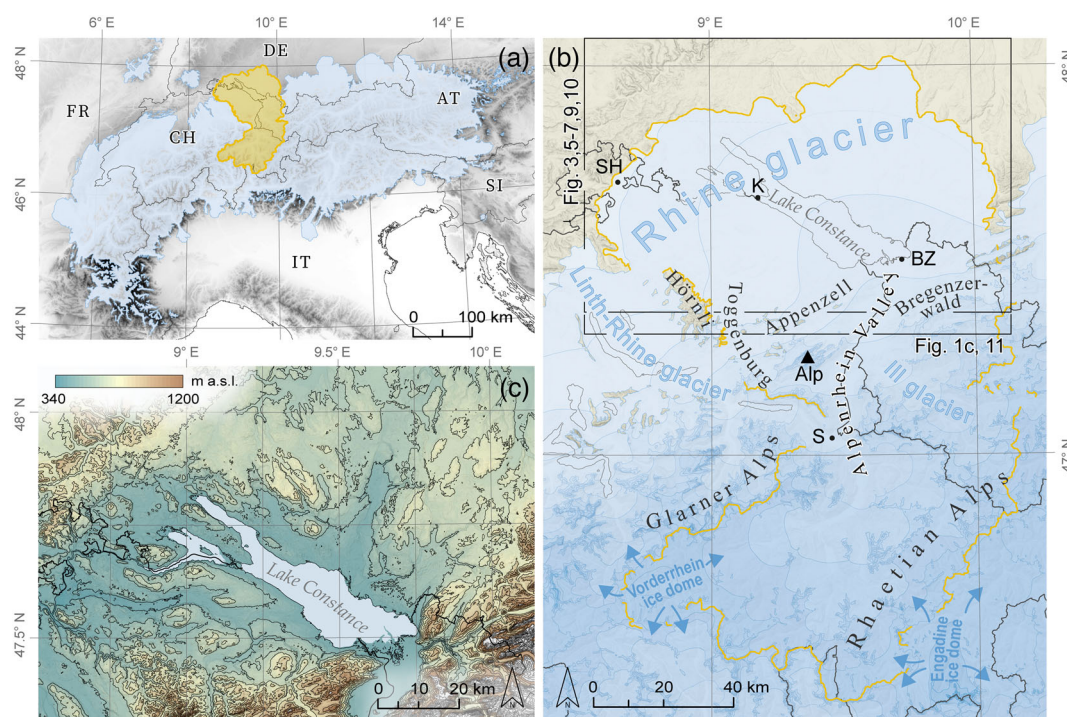


**FIGURE 1** (a) Last Glacial Maximum (LGM) maximum ice extents in the European Alps (modified after Bini et al., 2009). (b) LGM Rhine glacier system (modified after Ehlers et al., 2011) located in the central part of the Alps during the peak of the last glaciation. Flowing out of the high-elevation accumulation areas, including the Vorderrhein and Engadine ice domes (Florineth & Schlüchter, 1998), Rhine glacier ice was channelled northwards along the confined Alpenrhein Valley. At Sargans, ice diverged to the west and formed the Linth–Rhine glacier together with ice masses from the western Glarner Alps. At the mouth of the Alpenrhein Valley, the main Rhine glacier spread along the basin of Lake Constance and terminated as wide piedmont lobe. Alp, Alpstein massif (up to ~2500 m a.s.l.); BZ, Bregenz; K, Konstanz; S, Sargans; SH, Schaffhausen. (c) Elevation map of the area formerly covered by the LGM Rhine piedmont lobe (figure extent indicated in Figure 1b). Elevations between 340 and 1200 m a.s.l. are colour coded. Lake level of Lake Constance lies at 396 m a.s.l. Contour lines (black thin lines) with 100-m spacing, black thick lines indicate country borders. Elevation data provided by the European Union, Copernicus Land Monitoring Service 2020, European Environment Agency. [Color figure can be viewed at [wileyonlinelibrary.com](https://onlinelibrary.wiley.com/doi/10.1002/esp.5733)]

### 3 | METHODS

#### 3.1 | Geomorphological mapping

##### 3.1.1 | Data

The applied mapping approach is based on visual recognition and direct on-screen digitization of identified landforms in a GIS environment (Figure 2a–e). High-resolution elevation data are the prime source used and were provided by the Swiss Federal Office of Topography swisstopo, the State Agency for Spatial Information and Rural Development Baden-Württemberg, and the Bavarian Agency for Digitisation, High-Speed Internet and Surveying. SwissALTI<sup>3D</sup> is the open-access, high-resolution DEM of Switzerland and Liechtenstein. Areas covered by the new generation of SwissALTI<sup>3D</sup>, those include the study area, are characterized by an increased resolution of 0.5 m (Swisstopo, 2018b). Access to the light detection and ranging (LiDAR)-based 1-m relief model of Baden-Württemberg was gained through a fee-based Web Map Service (WMS). Elevation data from the openly available European DEM (EU-DEM 1.1; 25-m resolution; European Environment Agency, 2017) were used to complement the relief map. High-resolution elevation data (1 m) were purchased for the Bavarian parts of the study area. In light of potential azimuth bias affecting landform recognition (Smith & Clark, 2005; Wagner, 2017), relief shaded visualizations were generated using different single and multi-directional illumination angles. Where applicable, azimuth bias-free datasets (aspect, slope and aspect-slope) were created additionally (Figure 2). Hillshade images, slope and aspect layers were derived using Esri ArcGIS Spatial Analyst extension. The aspect-slope layer was created using ArcGIS raster functions. Modification of digital elevation data, including resampling to a

consistent raster resolution (1 m) and transformation to a uniform coordinate system, was undertaken. High-resolution aerial images supported mapping tasks additionally and were accessed via the public WebGIS applications or WMS servers.

Complementing remotely sensed elevation data, geological maps provided valuable insights. The Swiss GeoCover datasets, available through the Swiss Federal Office of Topography, offer standardized and homogenized geological vector information at scale of 1:25 000 (Strasky et al., 2016). A harmonized vector dataset on the geology of Baden-Württemberg at scale of 1:50 000 was provided by the State Office for Geology, Natural Resources and Mining (Regierungspräsidium Freiburg Landesamt für Geologie, 2013). The Bavarian Environment Agency publishes the vector datasets of the Geological Map of Bavaria, 1:25 000, under the Creative Commons licence. The geological maps present the aerial distribution of unconsolidated sediments and bedrock at the surface of the study area. In the public datasets, Quaternary depositional environments are further distinguished into, for example, aeolian, glacial, (glacio)fluvial and (glacio)lacustrine sediments. Displayed tectonic lineaments and solid and structural geological features provide additional guidance in areas where bedrock is shallow, and alternative interpretations for landform development must be considered. Multiple field visits to the study area were undertaken, but not every single landform was checked in the field (whether unconsolidated sediment or bedrock). To compensate for that, we prioritized information from field-based geological maps over the impression from remotely sensed data. Consequently, our mapped dataset does not include landforms that consist primarily of bedrock, even when they resembled streamlined subglacial features. They likely are streamlined bedrock. Ultimately, published literature and in particular explanatory notes on geological map sheets supported mapping procedure in the form of specific sediment description.

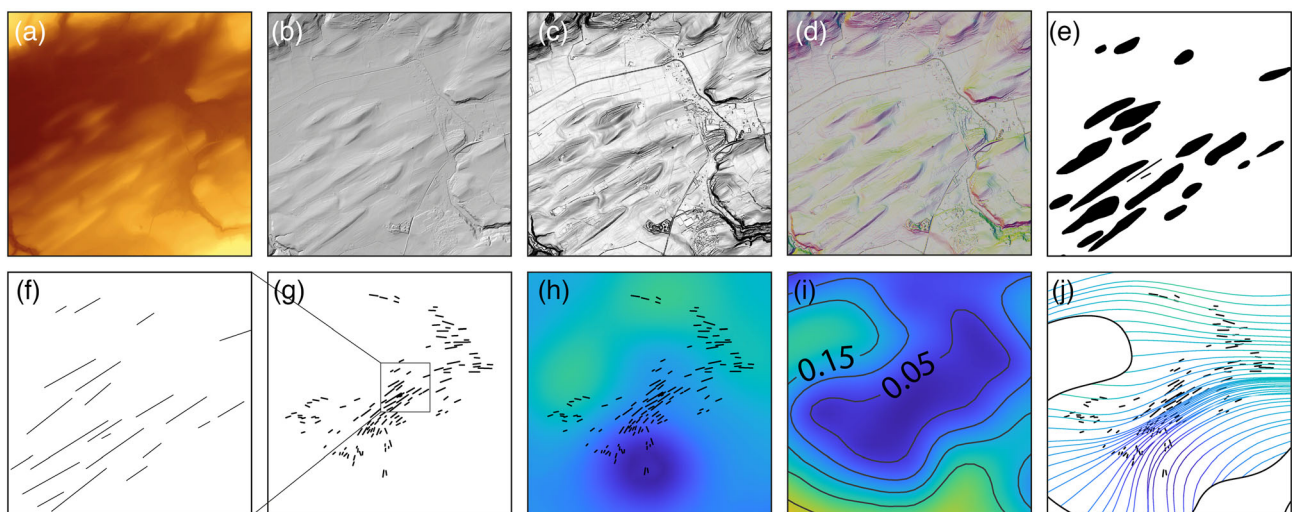


**FIGURE 2** Work flow applied in this study exemplified on the basis of a  $3 \times 3$ -km-sized area located in the southwestern part of the Rhine glacier piedmont lobe (ice flow direction is from northeast to southwest): (a) elevation data and its derivatives build the basis for geomorphological mapping of glacial and subglacial landforms (Table 1) on the Rhine foreland. A combination of (b) hillshade, (c) slope and (d) slope-aspect rasters was found most effective for mapping of (e) (sub)glacial landforms. (f) Mapped orientations of drumlins and glacial lineations are combined to (g) an isochronous flowset that builds the basis for the geostatistical interpolation of (h) basal flow fields, following the code of Ng and Hughes (2019). (i) The standard deviation of the kriged flow field is used to reject areas of high uncertainties and demarcate (e) reconstructed basal paleo-flow lines. [Color figure can be viewed at [wileyonlinelibrary.com](http://wileyonlinelibrary.com)]

### 3.1.2 | Mapping procedure

We mapped the following glacial and subglacial landform types: ice marginal areas (including moraine crests), ice decay areas, subglacial ribs, drumlins (including drumlin orientations) and glacial lineations based on the attributes listed in Table 1. Depending on the type of landform, digitization was carried out using polygons (drumlins, subglacial ribs and ice marginal areas) and line features (drumlin direction, glacial lineations and moraine crestlines). The direction of drumlins and glacial lineations was digitized in direction of paleo-ice flow (upstream to downstream), which is important for the subsequent calculation of landform direction (see also below). Ice marginal landforms include moraine ridges and mounds as well as hummocky and kettled terrain. Correlation of ice marginal deposits across the study area and beyond gaps in the geomorphological record was done under careful consideration and on the basis of landform position, elevation and relation to other geomorphic features (e.g., meltwater channels). When observed isolated from ice marginal areas, ice decay features, such as hummocky terrain, kettle holes or eskers, were recorded as separate landform category (ice decay area). Drumlin and subglacial ribs were delineated based on breaks of slope and under consideration of closed-loop contours. A combination of slope and aspect-slope layer was found to be most efficient in detecting and mapping landforms (Figure 2d). This is mainly for the accentuated breaks in slope, the contour lines displayed along with the aspect-slope image that highlight the transition from the respective landform to its surroundings, and for the prevention of azimuth bias. Drumlin direction was recorded for all drumlins except for those that lacked a clear longitudinal axis and hence did not allow assessing a unique flow direction, for example, circular or near-circular drumlins, drumlins with strong anthropogenic overprint or erosional drumlin remnants. Mapping was executed type by type, from west to east and north to south

such that multiple passes over the study area were ensured. In large parts, mapping has been performed at a scale of  $\sim 1:3000$ . After completing the first mapping pass, a second run was undertaken in order to account for gained mapping experience and to ensure uniformity in light of an evolving mapping technique. Mapping results have been regularly discussed in group with emphasis on ambiguous landforms or complex geomorphological situations. Mapping tasks were performed in Esri ArcMap 10.6.

Landform mapping by the use of remotely sensed data bases on the critical assumption that morphology alone can be used to recognize, delineate and classify landforms (Hughes et al., 2010). Unquestionably, missing insights on sedimentological structure of mapped landforms is a drawback of the applied approach and introduces uncertainties regarding landform genesis (cf. Boyes et al., 2021; Greenwood & Clark, 2009; Hughes et al., 2014). It seems improbable that greater spatial resolution would lead to the recognition of more subglacial and glacial landforms (Napieralski et al., 2007; Napieralski & Nalepa, 2010). The used high-resolution DEMs likely display the full preserved glacial and subglacial landform ensemble on land. Lastly, differences in mapper capabilities exist, but a comparative study on manual mapping of drumlins found that variations by a single interpreter can be relatively low (Hillier et al., 2015) and may be contained by following best practice routines (Chandler et al., 2018; Wagner, 2017).

### 3.1.3 | Morphometrics

Drumlin length, width and their respective ratio were derived on the basis of the ArcGIS 'Minimum Bounding Geometry' tool. Output of the tool additionally gave the start- and end-point coordinates and orientations of the longest possible line that can be drawn inside each

**TABLE 1** Mapped glacial and subglacial landforms and their main characteristics and identification criteria.

Landform type	Landform characteristics and identification criteria	Mapping style
Drumlin	Smooth, streamlined hill, aligned in direction of ice flow. Classically, elliptical or oval-shaped, with a steep stoss and a gentle lee end but also commonly found with symmetric or reversed asymmetric planar shape (Spagnolo et al., 2010). Drumlins often occur spatially organized in swarms or fields with individual landforms ranging in the order of $10^2$ to $10^3$ m in length and $10^1$ m in height (Bennett & Glasser, 2009; Clark et al., 2009).	Shape: Break-of-slope outline of individual landform. Direction: Crestline of individual landform.
Glacial lineation	Narrow, elongated, streamlined landform shaped in direction of ice flow (Clark, 1993; Spagnolo et al., 2014). Typically observed in close relationship to drumlins. Individual lineations may reach up to several kilometres in length.	Direction: Crestline of individual landform.
Subglacial rib (Rogen/ribbed moraine)	Transverse ridge characterized by an undulating crest with wavelengths of tens to thousands of metres and separated by troughs of similar spacing. Subglacial ribs often occur in fields. They are commonly drumlinized and/or are found in close spatial relationship to drumlins and MSGLs (Dunlop & Clark, 2006). Dissection by post-glacial processes is possible (Hughes et al., 2010).	Shape: Break-of-slope outline of individual landform.
Ice marginal area	Ridge-shaped or hummocky glacial landform; often forming continuous and undulating strings/bands along former ice margins of hundreds of metres width and include areas of irregular mounds and enclosed hollows. Moraine ridges may occur isolated and be segmented or eroded by post-depositional processes. Outside of forested areas often smooth in appearance.	Shape: Break-of-slope outline of individual landform. Ridged moraine: Crestline of individual landform.
Ice decay area	Isolated area of chaotic, hummocky terrain lacking moraine ridges, often with kettled morphology; typically found in basins or on flat outwash plains (i.e., pitted outwash). May include eskers.	Shape: Border of area covered.

Abbreviation: MSGLs, mega-scale glacial lineations.

mapped feature ('calculated orientation'; cf. Hughes et al., 2014; Spagnolo et al., 2011). The compass angle of both the manually mapped drumlin orientations and the mapped glacial lineations was extracted using the ArcGIS tool 'Linear directional mean'. Comparison of mapped and calculated drumlin orientations resulted in a median (mean) variation of 4° (6°). In 80% of the observation, mapped and calculated drumlin orientations varied by less than 9°. Output of the 'Linear directional mean' tool further informs on the circular variance within drumlin swarms. Circular variance measures the variation from the mean orientation and ranges between 1 and 0, whereby low values indicate homogenous landform orientations. Proximity analysis within single drumlin fields was performed using the 'Near tool'.

### 3.2 | Flowset delineation

Study and interpretation of basal flow patterns are based on the assignment of flowsets (Clark, 1999; Clark et al., 2000; Greenwood & Clark, 2009; Hughes et al., 2014; Kleman et al., 2007; Kleman & Borgström, 1996). Flowsets are discrete, coherent groups of landforms characterized by similar orientation and morphology as their neighbours (Clark, 1999; Clark et al., 2000). Isochronous flowsets are characterized by consistent 'rubber-stamped imprint' of bedforms and provide a single snapshot in time (Clark, 1999; Clark et al., 2000; Greenwood & Clark, 2009; Stokes & Clark, 2001; Wagner, 2017). Time-transgressive flowsets build up incrementally under varying flow. Cross-cutting or overprinted bedforms are left behind and exhibit a 'smudged' pattern due to constant modification. The morphology and orientation of a time-transgressive flowset will be less consistent (Clark, 1999; Clark et al., 2000; Greenwood & Clark, 2009; Hughes et al., 2014; Wagner, 2017). Our mapped drumlins and glacial lineations are visually generalized and delineated into flowsets. We do not include subglacial ribs in the delineated flowsets but use directional information from superimposed drumlins whose orientations are roughly perpendicular to the orientations of the underlying subglacial ribs.

### 3.3 | Inferring patterns of basal ice flow

Ng and Hughes (2019) recently proposed a quantitative approach to infer continuous basal ice flow patterns (flow fields) from defined subglacial landform flowsets using a kriging interpolation method (Figure 2). The herein implemented MATLAB workflow (Ng & Hughes, 2019) was specifically designed for deriving continuous flow fields from subglacial orientations. In a first step, orientation data of a flowset are compiled in an experimental variogram, which visualizes the semi-variance ( $\gamma$ ) between all possible data pairs as function of their separation distance ( $h$ ). To avoid data scatter, observations are grouped in equal-distant bins. Statistical correlation between the orientation of data pairs decreases with increasing distance. Thus, nearby observations receive higher weighting in the kriging process. This relation is translated to a kriging range  $R$  beyond which observations are excluded from the interpolation. In a variogram with a well-defined sill, the  $R$  value is chosen on the shoulder of the sill's rise. To guide the kriging process, we fit our model

variogram using the equations presented by Ng and Hughes (2019) that combine a linear component and a Gaussian component and is defined as follows:

$$\gamma(h) = C_0 + C_1H + C_3 \left[ 1 - e^{-\left(\frac{h}{C_4}\right)^2} \right],$$

where

$$H = \sqrt{h^2 + C_2^2} - C_2.$$

To improve and speed up the curve-fitting process, in light of the multiple combinations of kriging ranges and sills tested, we implemented an additional python script. This included a curve-fitting function from the scipy library (scipy.optimize.curve\_fit, [scipy.org](https://docs.scipy.org/doc/scipy/reference/optimize/curve_fit.html)) and uses least squares (lm, Levenberg–Marquardt) or trust region reflective (trf) algorithms to fit the equation parameters ( $C$  values; see Ng & Hughes, 2019). Kriging output will be most sensitive to the rise of the model variogram curve close to  $h = 0$ , while fitting at higher  $h$  values will have weaker influence (Ng & Hughes, 2019). To account for higher kriging weights at low  $h$  values, we experimented with different  $h_{\max}$  values to ensure best representation of the model variogram in the range up to and slightly beyond the sill.  $C_2$  was described as the parameter most sensitive in the fitting (Ng & Hughes, 2019) and was used to calibrate the model variogram to the lowest kriging residuals and root-mean-square (RMS) error (see also below). During kriging interpolation, the orientation value at any position within the defined domain is predicted as the linearly weighted sum of neighbouring observations up to the defined kriging range  $R$  (Ng & Hughes, 2019). Weighting is thereby constrained by the model variogram. The interpolation error is estimated by the kriging variance and translated to a standard deviation error in degrees that can be used to assess the reliability of the kriged field (see Ng & Hughes, 2019). Deviations will be lowest in areas densely covered with observations and highest at the borders of the model domain. The code of Ng and Hughes (2019) additionally provides cross-validation of kriging results by removing a single observation from the flowset at a time and using the remaining observations to predict its value. Residuals of kriged flow direction at the position of mapped lineaments provide an estimate for the overall success of the reconstruction. Distribution, RMS error and mean of residuals are used to optimize kriging by tuning initial input parameters ( $C_0$ – $C_4$ ,  $R$  and  $h_{\max}$ ) to achieve best reconstructions.

## 4 | RESULTS

The mapped subglacially streamlined landforms of the former Rhine glacier occur in a 20- to 30-km-wide band around Lake Constance (Figure 3). A total of 2460 drumlins (Figure 4a,b), 81 glacial lineations (Figure 4c) and 36 subglacial ribs (Figure 4d) were mapped. The majority of mapped bedforms are clustered in fields (Figure 5). Calculated key drumlin morphometrics, such as L:W ratios (Figure 6), relief and proximity of features are given in Tables 2 and 3. Predominant landform orientations are listed in Table 4 and illustrated in Figures 7 and

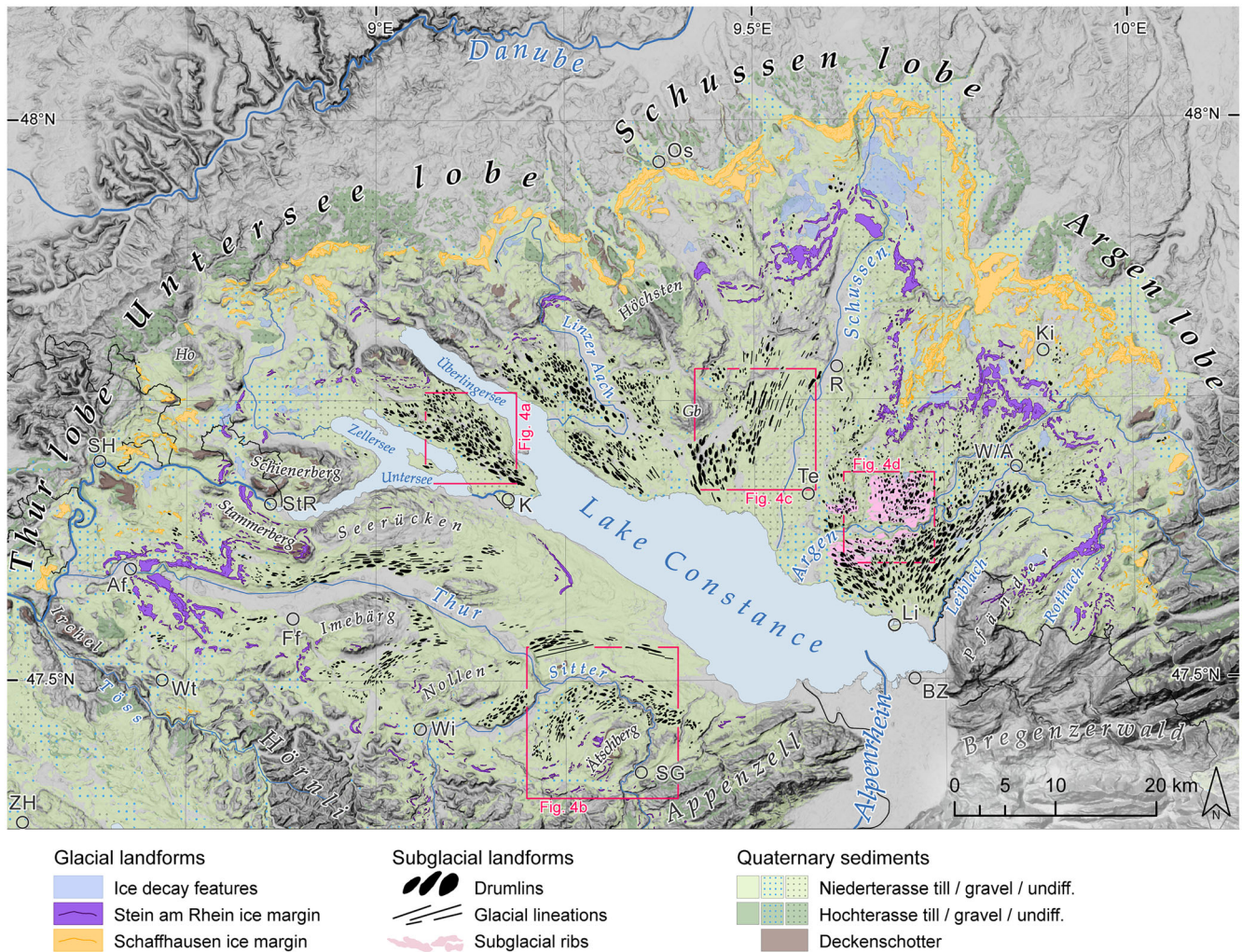


**FIGURE 3** Glacial geomorphological map of the piedmont lobe of the Last Glacial Maximum (LGM) Rhine glacier on the Swiss-German Alpine foreland mapped on the basis of digital elevation data (Figure 2 and Table 1). The majority of subglacially streamlined landforms are located internal to the Stein am Rhein ice margin, where they are organized in fields (see also Figure 5) radially around the Lake Constance basin. Geological units modified from the Geological Atlas of Switzerland (1:25 000; Eugster et al., 1960; Geiger, 1943, 1968; Haldimann et al., 2017; Hantke, 2003; Hofmann, 1981, 1973, 1967, 1993, 1997; Hottinger et al., 1970; Hübscher, 1961; Ludwig, 1930; Pavoni et al., 1992; Rey et al., 2011; Saxer, 1965; Wyssling, 2007; Zaugg, 2007; Zaugg & Geyer, 2008), the Geological Map of Baden-Württemberg (1:50 000; Regierungspräsidium Freiburg Landesamt für Geologie, 2013) and the Geological Map of Bavaria (1:25 000 provided by the Bavarian Environment Agency). Niederterrasse refers to Late Pleistocene sediments, and Hochterrasse and Deckenschotter refer to Middle Pleistocene and Early Pleistocene sediments, respectively (Graf & Burkhalter, 2016). Cities: Af, Andelfingen; BZ, Bregenz; Ff, Frauenfeld; K, Konstanz; Ki, Kißlegg; Li, Lindau; R, Ravensburg; SG, St. Gallen; SH, Schaffhausen; StR, Stein am Rhein; Te, Tettngang; W/A, Wangen im Allgäu; Wi, Wil; Wt, Winterthur; ZH, Zürich. Mountain peaks: Gb, Gehrenberg; Ho, Hohenstoffeln. Elevation data provided by the European Union, Copernicus Land Monitoring Service 2020, European Environment Agency. [Color figure can be viewed at [wileyonlinelibrary.com](https://onlinelibrary.wiley.com)]

8. From the 2460 mapped drumlins, we were able to determine 2288 subglacial orientation vectors. A total of 172 drumlins of near-circular shape or partially eroded bedforms lacked unambiguous crestlines and directions. Twelve drumlins were recorded in tributary valleys within the Bregenzerwald region (Figure 3) and are not further discussed here. On the basis of glacial inversion and diagnostic criteria (see Section 3.2), we differentiate two flowsets on the Rhine foreland: (i) the Schaffhausen flowset (fs SHmax) associated with the Schaffhausen ice margin and (ii) the Stein am Rhein flowset (fs StR) linked to the internal Stein am Rhein frontal moraines (Figure 9). Basal flow paths of fs SHmax were, due to the low number of single observations and spread-out nature of the flowset, visualized qualitatively. In the case of fs StR, we reconstructed an extensive flow field using the kriging routine of Ng and Hughes (2019).

#### 4.1 | Subglacial landforms of the Schaffhausen flowset

Scattered widely across the study area, 101 drumlins are located in between the frontal moraines of the LGM maximum ice margin (Schaffhausen stadial) and the late LGM Stein am Rhein stadial moraines (Figure 3). These drumlins are typically located several kilometres behind the outer LGM maximum moraines and are interpreted to have formed during the Schaffhausen stadial. Drumlins occur in all four main lobes of the former piedmont glacier, typically in loose groups of just a few; but isolated drumlins are present as well. The occurrence of drumlins is often restricted to higher parts of the landscape. Glacial lineations are missing from this outer zone. We mapped 18 drumlins within the swath covered by the Stein am Rhein

**FIGURE 4** Subglacial landforms on the Rhine foreland: (a) drumlins of Bodanruck drumlin field between Überlingersee and Zellersee. (b) Fürstenland drumlin field with landforms nestled up against and turning around the base of Ätschberg mountain. Ice flow direction from westsouthwest to south and therewith towards the Alpine mountain front. (c) Transition from drumlins to more elongated glacial lineations in the lower Schussen Valley. (d) Subglacial ribs within the Argen drumlin field to both sides of Argen River channel. Arrows indicate ice flow directions. For location of blow-ups, see Figure 3. [Color figure can be viewed at [wileyonlinelibrary.com](https://onlinelibrary.wiley.com)]

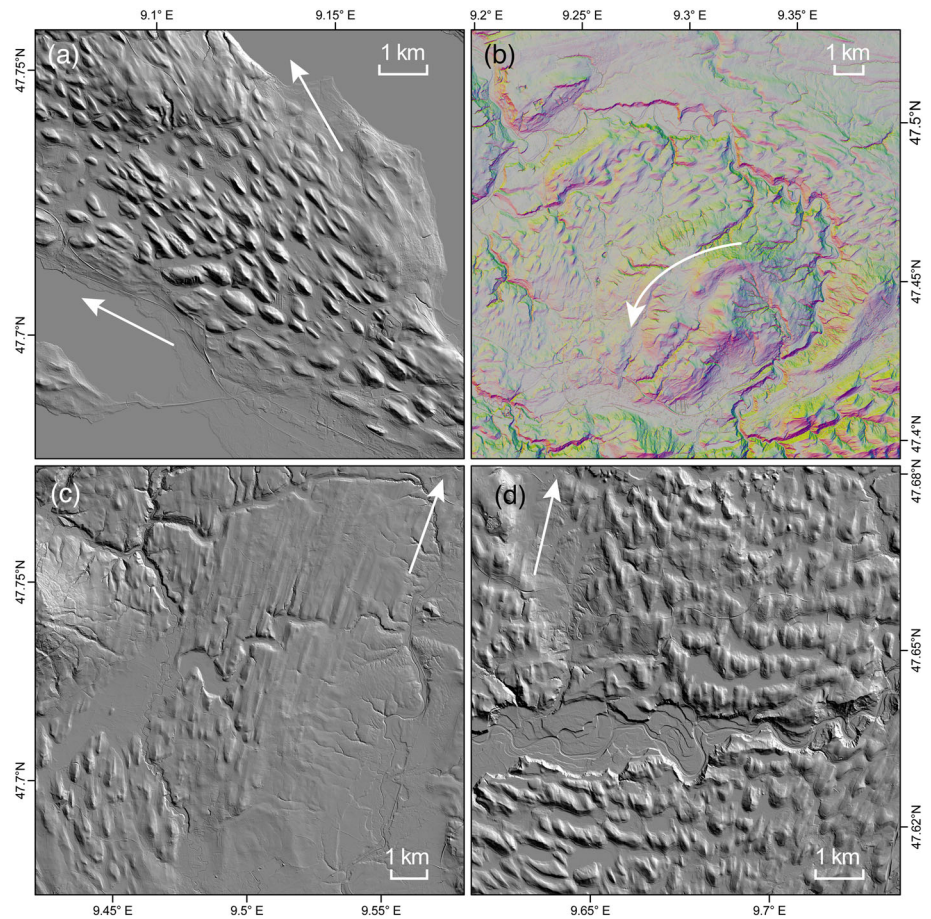
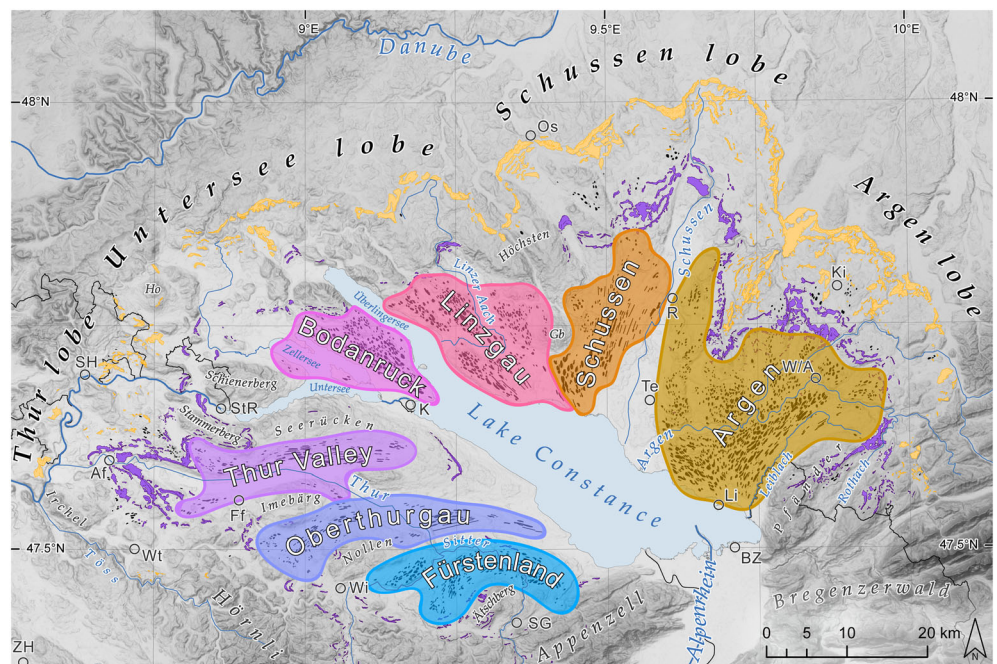


**FIGURE 5** The majority of subglacial landforms on the Rhine foreland occur in swarms internal to the Stein am Rhein ice margin and separated by areas where bedforms are lacking. Based on this spatial pattern, seven drumlin fields were differentiated, from west to east: Fürstenland, Oberthurgau, Thur Valley, Bodanruck, Linzgau, Schussen and Argen fields. Ice marginal deposits of Schaffhausen and Stein am Rhein stadials are shown in yellow and purple, respectively (Figure 3). For abbreviations of city and mountain names, see Figure 3. Elevation data provided by the European Union, Copernicus Land Monitoring Service 2020, European Environment Agency. [Color figure can be viewed at [wileyonlinelibrary.com](https://onlinelibrary.wiley.com)]



stadial frontal moraines (Figure 3). Based on the fact that drumlins of similar appearance and matching orientation are found just outboard of these moraines, we attribute these intramorainic drumlins to the Schaffhausen stadial.

Drumlins of the Schaffhausen stadial hold the smallest mean and median lengths and lowest L:W ratios (Table 2) of all drumlins in this study. Their relief is on the lower end of the observed range on the

Rhine foreland. Drumlin directions vary from southsouthwest to east-northeast with the majority of features being oriented between westsouthwest and northnortheast (Figures 7 and 8 and Table 4).

Four small-scale flow subsets (fs SHmax a-d) were discerned within the LGM maximum drumlins (Figure 9); not every bedform was assigned to one of the flow subsets. Each of the four flow subsets is made up of 12–28 individuals, summing up to a total of 71 drumlins

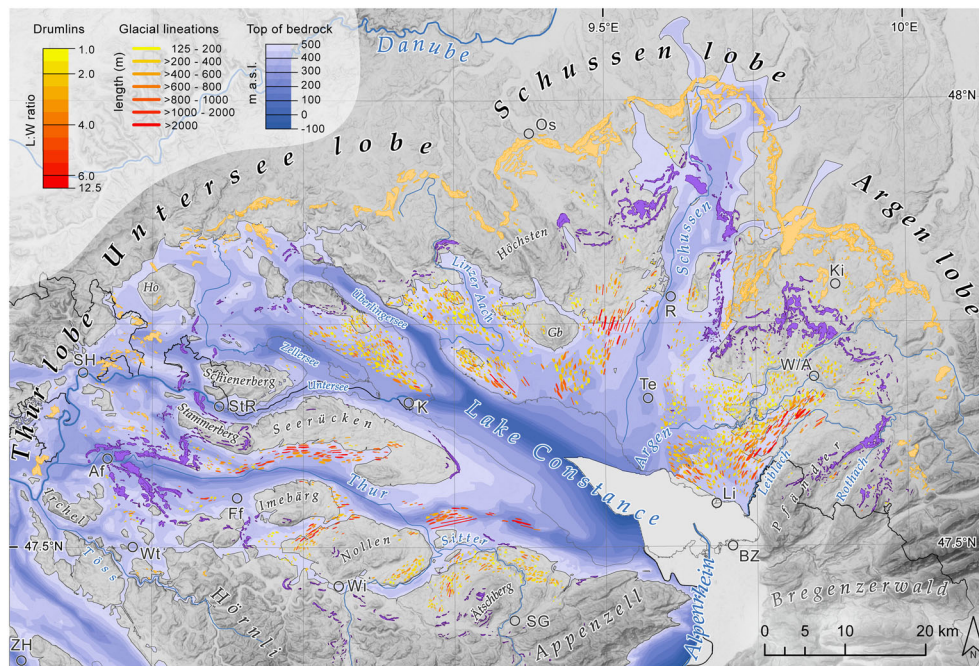


**FIGURE 6** Elongation ratios and lengths of drumlins and glacial lineations on the foreland of the Last Glacial Maximum (LGM) Rhine glacier compared to modelled top of bedrock elevations (GeoMol Team, 2015; Swisstopo, 2018a). Bedrock elevations from  $-100$  to  $500$  m a.s.l. are colour coded in blue. Highly elongated bedforms are thought to indicate zones of higher basal velocities (Barchyn et al., 2016; Stokes & Clark, 2001, 2002; Stokes, Spagnolo, et al., 2013). Elongated drumlins and longer glacial lineations align with the existing, partly overdeepened basins and troughs (Ellwanger et al., 2011; GeoMol Team, 2015; Jordan, 2010; Pietsch & Jordan, 2014). Thur trough, Schussen trough and Leiblach trough underlie the present river valleys as labelled on the map. Troughs of Zellersee and Überlingersee follow the eponymous arms of Lake Constance. Mapped ice marginal deposits of Schaffhausen and Stein am Rhein stadials are shown in yellow and purple, respectively (Figure 3). For abbreviations of city and mountain names, see Figure 3. Elevation data provided by the European Union, Copernicus Land Monitoring Service 2020, European Environment Agency. [Color figure can be viewed at [wileyonlinelibrary.com](https://onlinelibrary.wiley.com)]

that comprise fs SHmax. The flow subsets are locally restricted and spread across the foreland, with up to several tens of kilometres separating them. We hence make no assumption on whether they were formed isochronously or time transgressively. Certainly, they must have formed during the LGM maximum phase (Schaffhausen stadial) and thus before the hereafter presented Stein am Rhein flowset. At the very western margin of the Rhine glacier, just north of Winterthur, drumlins of flow subset fs SHmax a, located in a 2- to 3-km-wide valley, point first in a southwesterly direction and then curve more towards the south. On the right side of the Thur Valley, near Andelfingen, fs SHmax b is northwest directed (Figure 9). In the eastern part of the Schussen lobe ( $\sim 5$ – $8$  km upstream of the terminal moraines of Ostrach), bedforms of fs SHmax c are streamlined in a northnorthwest direction. Fs SHmax d is located in the eastern sector of the study area  $\sim 6$  km upstream of the outer Schaffhausen moraines in the Argen lobe and records northeast orientations.

## 4.2 | Subglacial landforms of the Stein am Rhein flowset

The vast majority of mapped drumlins ( $n = 2329$ ), all glacial lineations and all subglacial ribs are located upstream of the Stein am Rhein ice marginal complex and are organized into swarms or fields (Figure 5). Drumlins occur up to a few hundreds of metres to the inner Stein am Rhein frontal moraines. Subglacial landforms are nearly completely restricted to elevated surfaces above the present-day drainage

network and in case of Thur and Schussen valleys also to steeper valley slopes (Figure 3). On the basis of their geographical distribution, directional and morphological similarities, we distinguished seven drumlin fields (from west to east): Fürstenland, Oberthurgau, Thur Valley, Bodanruck, Linzgau, Schussen and Argen fields. Single drumlin fields are mainly separated by incised river valleys or areas where subglacial bedforms are lacking (e.g., along valley bottoms) or potentially submerged (e.g., Überlingersee).

The number of drumlins is unequally distributed across the foreland area and single drumlin fields. Nearly two thirds of mapped drumlins are located east of Lake Constance. The drumlin fields of Bodanruck, Linzgau and particularly Argen are characterized by close spacing of single features (Table 3). The median distances to the closest neighbouring drumlin are 62, 59 and 36 m, respectively. The Thur Valley and Oberthurgau drumlin fields are less densely populated with largest median distances to the next closest drumlin of 112 and 97 m. Relief of single drumlins ranges from a few metres up to 60 m with median heights of 11–16 m (Table 2). The tallest drumlins are found in the central parts of the Rhine piedmont lobe (Bodanruck and Linzgau fields). Median drumlin lengths range from  $\sim 310$  to 450 m (Table 2). Highest median length occurs in the Thur Valley, followed by the Schussen Valley. Differences between drumlin fields are smaller with regard to drumlin width. Median widths of single fields range from 125 to 164 m. Drumlin fields in the west have a tendency to slightly narrower drumlins. These observations manifest in generally higher L:W ratios in the drumlin fields west of Lake Constance (median L:W ratios of 3.3 and 2.9 for Oberthurgau and Thur Valley

TABLE 2 Morphometrics of drumlins and glacial lineations.

Drumlin field	Drumlins						Glacial lineations					
	Length		Width		L:W ratio		Relief		Number		Length	
	Range m	Median (mean) m	Range m	Median (mean) m	Median (mean) m	Median (mean) m	Range m	Median (mean) m	Number m	Number m	Range m	Median (mean) m
LGM maximum: Schaffhausen stadial												
External Stein am Rhein ice margin	101	102–612	287 (301)	53–355	153 (162)	1.8 (1.9)	4–33	11 (12)	-	-	-	-
In-between Stein am Rhein ice margin	18	99–426	177 (205)	68–160	101 (107)	1.7 (1.9)	6–18	11 (12)	-	-	-	-
Late LGM readvance: Stein am Rhein stadial												
Rhine west	245	119–964	309 (346)	59–312	145 (155)	2.2 (2.3)	4–41	13 (15)	3	189–844	758 (688)	
Oberthurgau	145	106–2450	363 (456)	61–312	125 (136)	2.9 (3.3)	4–44	11 (13)	17	126–5735	328 (976)	
Thur Valley	144	119–1813	453 (516)	44–342	134 (147)	3.3 (3.6)	5–56	13 (15)	19	226–1259	501 (590)	
Rhine centre	271	71–1192	361 (388)	42–439	154 (166)	2.3 (2.5)	4–58	16 (19)	-	-	-	-
Linzgau	395	103–1554	340 (381)	39–502	161 (172)	2.2 (2.3)	3–62	16 (18)	5	378–2491	939 (1107)	
Rhine east	190	134–1854	388 (484)	55–437	164 (180)	2.4 (2.8)	3–46	12 (14)	31	271–2157	649 (758)	
Argen	939	77–1797	313 (371)	38–355	152 (164)	2.0 (2.3)	3–58	14 (16)	6	321–1221	683 (742)	
Tributary valleys	12	197–653	287 (341)	83–205	158 (147)	2.2 (2.4)	6–19	15 (14)	-	-	-	-

Abbreviation: LGM, Last Glacial Maximum.

**TABLE 3** Proximity of neighbouring drumlins.

Drumlin field	Drumlins			
	Number	Distance to closest neighbour		
		Range m	Median (mean) m	
LGM maximum: Schaffhausen stadial				
External Stein am Rhein ice margin	101	1–14 817	150 (821)	
In-between Stein am Rhein ice margin	18	18–7387	87 (509)	
Late LGM readvance: Stein am Rhein stadial				
Rhine west	Fürstenland	245	0–1193	79 (108)
	Oberthurgau	145	8–949	97 (144)
	Thur Valley	144	2–2277	112 (116)
Rhine centre	Bodanruck	271	0–1012	59 (97)
	Linzgau	395	0–592	62 (99)
Rhine east	Schussen	190	0–810	83 (126)
	Argen	939	17–129	36 (45)
Tributary valleys	Bregenzerwald	12	52–2857	128 (657)

Abbreviation: LGM, Last Glacial Maximum.

**TABLE 4** Orientation of drumlins and glacial lineations.

Drumlin field	Drumlins				Glacial lineations		
	Number	Linear directional mean		Circular variance Degree	Number	Linear directional mean	
		Degree				Degree	
LGM maximum: Schaffhausen stadial							
External Stein am Rhein ice margin	95	331		0.39	-	-	-
In-between Stein am Rhein ice margin	15	287		0.04	-	-	-
Late LGM readvance: Stein am Rhein stadial							
Rhine west	Fürstenland	229	230	0.09	3	222	0.06
	Oberthurgau	142	243	0.10	17	245	0.14
	Thur Valley	139	269	0.05	19	265	0.01
Rhine centre	Bodanruck	263	315	0.03	-	-	-
	Linzgau	373	326	0.04	5	321	0.00
Rhine east	Schussen	184	7	0.05	31	17	0.01
	Argen	837	11	0.16	6	59	0.00
Tributary valleys	Bregenzerwald	11	47	0.05	-	-	-

Abbreviation: LGM, Last Glacial Maximum.

fields, respectively) compared to central (median L:W ratio of 2.3 for Bodanruck field) and eastern parts (median L:W ratio of 2.0 for Argen field) of the Rhine system (Table 2). High L:W ratios are found parallel to the major foreland troughs, for example, the Thur and Schussen valleys. Subglacial bedforms with low L:W ratios or near-circular shape further occur in proximity of the former Stein am Rhein ice margin (Figure 6).

Glacial lineations are distributed roughly equally in the eastern and western parts of the former lobe but are missing in the Bodanruck field. Mapped glacial lineations range from few hundreds of metres up to 5.7 km in length (Table 2). The longest ~20% of glacial lineations mapped in the study area reach lengths above 1 km. Roughly 5% are

longer than 2 km. The longest lineations are found in the eastern part of the Oberthurgau and Linzgau fields (Figure 6).

High (~20–50 m) ridges with undulating crestlines were identified in an ~60-km<sup>2</sup>-sized area on both sides of the Argen River (Figures 3 and 4d). These ridges are typically 3–9 km long, ~200–850 m wide and 100–500 m apart. Single ridges may be dissected but can also be clearly connected. Horns are found on the downglacier side (cf. Sutinen et al., 2010) but occur infrequently. The ridges trend east–west and, therefore, roughly perpendicular to the orientation of surrounding and superimposed drumlins. The latter however are often characterized by near-circular shape and lack clear crestlines. We interpret these ridges as subglacial ribs (Rogen/ribbed moraines

[Clark, Ely, Greenwood, et al., 2018; Dunlop & Clark, 2006; Knight & McCabe, 1997]; see Table 1).

Orientation of streamlined bedforms internal to the Stein am Rhein frontal moraines follows an overall radial pattern (Figures 7 and 8 and Table 4). The drumlin fields of Fürstenland and Oberthurgau feature south, southsouthwest and west oriented landforms. Drumlins and glacial lineations of the Thur Valley field face westsouthwest, west and westnorthwest. Westnorthwest, northwest and northnorthwest orientations are shown by the subglacially streamlined bedforms from the Bodanruck and Linzgau fields, while north, northnortheast and northeast orientations are covered by bedforms of the Schussen and Argen fields. With regard to bedform orientation, the most striking feature of the study area is the distinct curve displayed by the Fürstenland field bedforms (Figure 4b). Orientations shift from west tending to clearly southsouthwest and south facing in the downglacier direction (Figure 7). A similar curve is seen, but in an attenuated way, in the Oberthurgau drumlin field to the north.

Low circular variance values found in Bodanruck (0.03), Linzgau (0.04), Schussen Valley (0.05) and Thur Valley (0.05) indicate drumlin fields with homogenous landform orientations (Figure 8). Extensive fields such as the Argen (0.16) with greater directional variations or fields with turning flow directions (Oberthurgau [0.10] and Fürstenland [0.09]) are characterized by higher variance values.

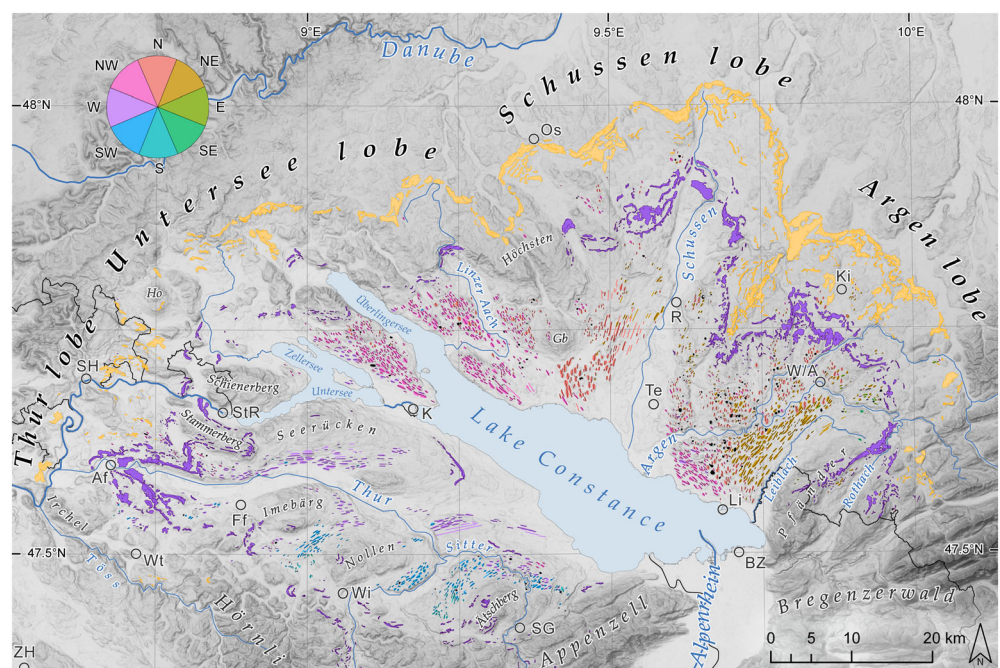
All drumlins and glacial lineations of the drumlin fields upstream of the Stein am Rhein ice margin are integrated into a single flowset: fs StR (Figure 9). Based on geomorphological observations plus the criteria defined by Clark (1999), Clark et al. (2000), Greenwood and Clark (2009), Hughes et al. (2014) and Stokes and Clark (2001), we assess fs StR to have formed isochronously. The mapped subglacial features have clear ('rubber-stamped') appearance and are not smudged. We fail to see any abrupt changes in landform morphology. No beheading and very few instances of cross-cutting are observed. In the rare cases of superimposition, overlapping drumlins point in the same direction. Nonetheless, in some areas, adjacent drumlins exhibit minor variations in direction (Figure 7), while sharing similar

morphology and appearance with neighbouring drumlins. We found little geomorphological evidence of renewed readvance or prolonged glacier stabilization upstream of the Stein am Rhein stadial moraines. We mapped a single SE–NW trending left-lateral moraine about 2–3 km south of Lake Constance (Figure 3). This moraine, ascribed to the Konstanz stadial (Keller & Krays, 2005; Schmidle, 1916), has been linked to sedimentological evidence in cores from the city of Konstanz that point to a glacier halt during lake filling (Zaugg et al., 2008). The presence of a grounding-line fan (cf. Fitzsimons & Howarth, 2017) during active retreat is suggested. Important for our study is the fact that we could not identify any moraines that crosscut the Stein am Rhein stadial drumlins. In addition, marked splaying patterns (fanning of orientations within a short distance) are only observed in close proximity to the Stein am Rhein ice margin but are absent further upstream. No swath-like changes in orientations of drumlins and glacial lineations, which would indicate readjusting of basal ice flow as the ice margin retreats, are observed. As we find no clear evidence for several time periods of formation, we follow the simplest situation and interpret all subglacial landforms internal to the Stein am Rhein ice marginal complex to have been shaped at the same time (isochronous) during the late LGM readvance (Habbe, 1988; Kamleitner et al., 2023; Keller & Krays, 2005; Penck & Brückner, 1909).

### 4.3 | Modelled basal ice flow directions of the Stein am Rhein flowset

The kriging workflow of Ng and Hughes (2019) was applied to the 2248 directions of the Stein am Rhein flowset (fs StR). The experimental variogram of fs StR (Figure S1a) was compiled at a bin size of 1 km with a median of 65 000 observations per bin. The variogram curve shows a near linear rise with intervening smaller sills. This is likely due to the radial pattern of mapped orientations and the gaps between single drumlin fields. Consequently, we experimented with different *R* values. We find an *R* of 10 km corresponding to the first

**FIGURE 7** Spatial distribution of orientations of streamlined subglacial landforms (drumlins and glacial lineations) at the former bed of the Last Glacial Maximum (LGM) Rhine piedmont lobe. Directions among neighbouring bedforms are largely consistent. Ice marginal deposits of Schaffhausen and Stein am Rhein stadials are shown in yellow and purple, respectively (Figure 3). For abbreviations of city and mountain names, see Figure 3. Elevation data provided by the European Union, Copernicus Land Monitoring Service 2020, European Environment Agency. [Color figure can be viewed at [wileyonlinelibrary.com](https://onlinelibrary.wiley.com)]



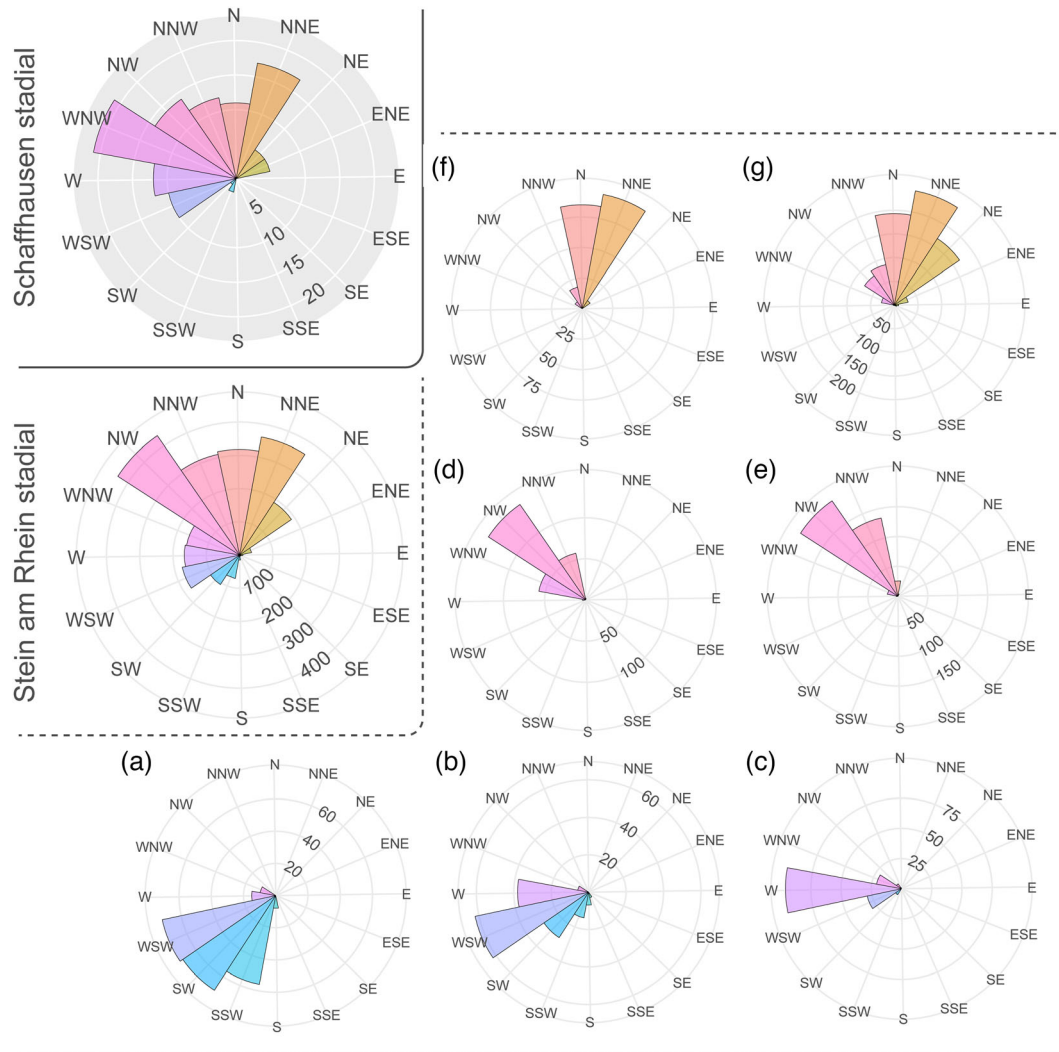


**FIGURE 8** Rose plots (two upper left plots) illustrating the orientations of drumlins and glacial lineations that formed while the glacier was at the Schaffhausen ice margin (Last Glacial Maximum [LGM] maximum; in grey) and while it was at the Stein am Rhein ice margin (late LGM readvance; in white). Rose plots for the seven Stein am Rhein stadal drumlin fields: (a) Fürstenland, (b) Oberthurgau, (c) Thur Valley, (d) Bodanruck, (e) Linzgau, (f) Schussen and (g) Argen. Location of single drumlin fields is shown in Figure 5. Segment length is scaled to the number of observations. Note the large variations in number of subglacial lineations between Schaffhausen and Stein am Rhein stadials and individual drumlin fields. [Color figure can be viewed at [wileyonlinelibrary.com](http://wileyonlinelibrary.com)]

variogram sill yielding kriging results with lowest residuals and RMS error, although very similar to an  $R$  value of 20 km at the shoulder of the second sill. Our best fit model for  $f_s$  StR uses the following constants:  $C_0 = 0.05$ ,  $C_1 = 0.004$ ,  $C_2 = 2.50$ ,  $C_3 = 0.19$  and  $C_4 = 5.44$  (see model function in Section 3.3). The RMS error is  $14^\circ$  (Figure S1b). Corresponding residuals hold mean values of  $0.1^\circ$  and are uncorrelated (Figure S1c).

Our dataset consists predominantly of orientations derived from drumlins (2167 vectors from drumlins in contrast to 81 from glacial lineations). From processing individual sections of the Stein am Rhein flowset separately, we realized that RMS errors increase from west to east, with the lowest RMS error of about  $11^\circ$  in the western part of  $f_s$  StR to the highest RMS error for the Argen region ( $\sim 17^\circ$ ). This trend possibly reflects the high number of closely spaced but comparably short drumlins in the Argen area and their small-scale variability in orientation compared to fewer, wider spaced and more strongly elongated drumlins and glacial lineations in the western lobes. Our observations agree with findings from Ng and Hughes (2019) that report residuals of drumlins to be generally larger than those for

MSGLs, indicating that drumlin directions are more irregular or kriging uncertainties are larger when inferring directions from them.

Spatial distribution of kriging standard deviation across the model domain is shown in Figure S2. In light of the obtained RMS error ( $14^\circ$ ), we use the  $15^\circ$  standard deviation contour to clip the kriged flow field and disregard the flowline reconstructions beyond this boundary (Figures 10 and S2). The  $15^\circ$  standard deviation contour of the flow field over large areas falls together with or runs in close distance to the corresponding Stein am Rhein ice margin. Conditioned by the spatial distribution of drumlins and glacial lineations and the chosen kriging range, this overlap provides additional and independent observations to evaluate the modelled paleo-ice flow directions.

Figure 10 shows the basal ice flow lines for the reconstructed flow field in comparison to our mapped LGM ice margins of the Schaffhausen and Stein am Rhein stadials and underlying topography. The interpolation reproduces the radial directions emanating from the Alpenrhein Valley outlet and fanning out to the margins well. Decreasing distance between flow lines indicates converging basal ice flow as constricted by topography. In contrast, increasing distance between

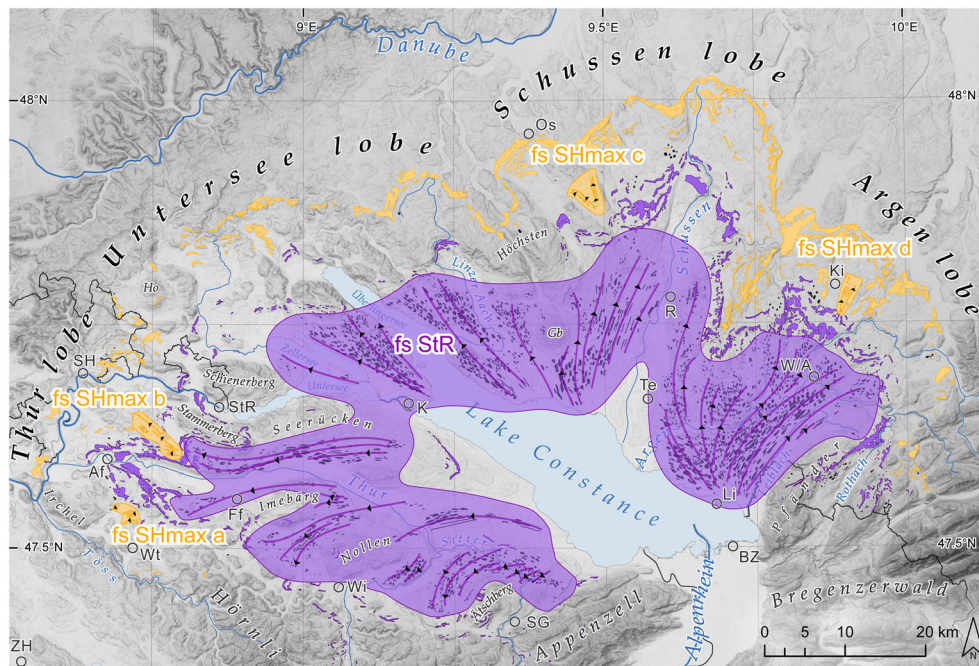


**FIGURE 9** Delineated flowsets of the Last Glacial Maximum (LGM) Rhine glacier foreland comprise streamlined bedforms associated with the Schaffhausen ice margin (fs SHmax) and the internal Stein am Rhein ice margin (fs StR), respectively. Fs SHmax and its four flow subsets (fs SHmax a–d) must have formed during the LGM maximum phase (Schaffhausen stadial). The upstream fs StR is interpreted to have formed isochronously during the late LGM readvance to and the subsequent stabilization at the Stein am Rhein ice margin. Flow lines are drawn manually. Mapped ice marginal deposits of Schaffhausen and Stein am Rhein stadials are shown in yellow and purple, respectively (Figure 3). For abbreviations of city and mountain names, see Figure 3. Elevation data provided by the European Union, Copernicus Land Monitoring Service 2020, European Environment Agency. [Color figure can be viewed at [wileyonlinelibrary.com](https://onlinelibrary.wiley.com)]

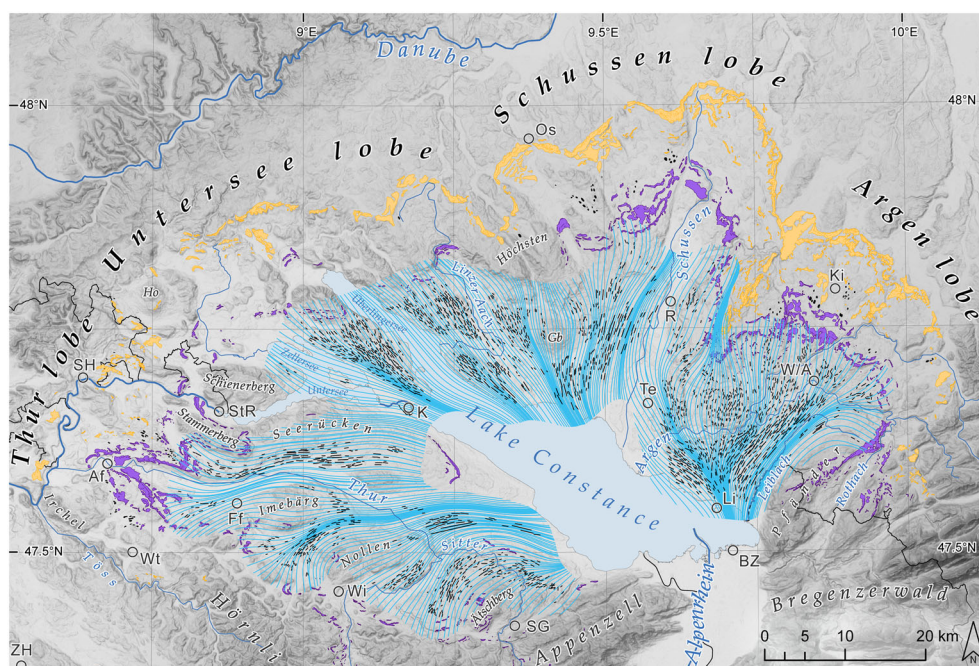


**FIGURE 10** Reconstructed basal paleo-ice flow trajectories (in blue) of the Rhine glacier during the late Last Glacial Maximum (LGM) readvance to the Stein am Rhein stadial moraines. Basal flow lines are based on the geostatistical interpolation of mapped drumlins and glacial lineations of fs StR (black ticks; Figure 9) following the code of Ng and Hughes (2019) and are cut off at the 15<sup>th</sup> kriging standard deviation contour (Section 3.3 and Figure S2). Note that the flow lines have not been clipped to the Stein am Rhein ice margin (Figure 11b). Fanning-out basal flow from the basin of Lake Constance is evident. Topographic control on basal ice flow patterns is well recognizable from diverging and converging flow paths, particularly in the southwestern parts of the foreland. Ice marginal deposits of Schaffhausen and Stein am Rhein stadials are shown in yellow and purple, respectively (Figure 3). For abbreviations of city and mountain names, see Figure 3. Elevation data provided by the European Union, Copernicus Land Monitoring Service 2020, European Environment Agency. [Color figure can be viewed at [wileyonlinelibrary.com](https://onlinelibrary.wiley.com)]

flow lines signifies diverging basal ice flow. Specific basal flow directions are discussed in detail in the next section in view of geomorphological evidence and suggested relative differences in basal ice flow velocities.

## 5 | DISCUSSION

### 5.1 | The Rhine glacier during the Schaffhausen stadial

During the LGM maximum (Schaffhausen stadial at 26–22 ka; Kamleitner et al., 2023; Preusser et al., 2007), Rhine glacier exited the Alps at the mouth of Alpenrhein Valley (Figure 1), where it had been laterally confined and strongly funneled. Upon encountering a much flatter landscape on the foreland, it spread to the west, north and east, filled the Lake Constance basin and, from there, flowed uphill (Figure 1c) to its maximum position at the Schaffhausen stadial moraines (Figure 11a). Further ice was contributed from independent

accumulation areas to the south, Toggenburg and Alpstein (Figure 1) in the western sector and Rothach tributary coming from Bregenzwald in the eastern sector (Figure 3) (Bini et al., 2009; Jäckli, 1962; Keller, 1981; Keller & Krays, 2005). In the zone proximal to the LGM maximum glacier front, orientation of the Schaffhausen stadial drumlins (flowset fs SHmax; Figure 9) yields information about basal ice flow. Cohen et al. (2018) presented fully coupled Stokes ice flow models (Elmer/Ice) of the Rhine glacier during the LGM. Their simulations aimed at reproducing the dynamics of the Rhine glacier at its maximum extent and would thus be comparable to our SHmax flowset.

The configuration of the Argen lobe moraines suggests the presence of two sublobes during the maximum extent, with a suture zone located west of Kißlegg (Figure 3). Flow in the frontal part of the Argen lobe was mainly to north-northeast as seen in the drumlin orientations (fs SHmax d) (Figure 9). This is similar to the model results of Cohen et al. (2018). Between the Argen and Schussen lobes, a huge interlobate complex developed (Figure 3; Kamleitner et al., 2023). The Argen–Schussen interlobate complex covers an area of approximately 13 km<sup>2</sup>, with a length of ~12 km and a width of up to 2 km. From the nearby meltwater channels to the top of the ridges, the relief is up to 100 m. Interlobate areas have been discussed at, for example, the Laurentide Ice Sheet (Carlson et al., 2005; Sookhan et al., 2018) and the Scandinavian Ice Sheet (Punkari, 1980, 1997). The elevations and arrangement of the suture zone suggest that the complex built up right after the glacier had pulled back from the outermost frontal moraines. Minimum ice surface levels during LGM maximum extent went from 770 m a.s.l. at the highest point of the Argen–Schussen suture zone to ~700 m a.s.l. at the ice front.

The moraine arc of the Schussen lobe during Schaffhausen stadial juts several kilometres forwards in comparison to the frontal sector of the Argen lobe to the west. This underscores the likely presence of faster flowing ice as a consequence of the presence of the Schussen trough (Figure 6; see also below) (cf. Jennings, 2006; Mooers, 1989; Szuman et al., 2021). The Cohen et al. (2018) models show a slightly more northward flow path than the north-northwest directed basal flow pattern we see in fs SHmax c.

Only isolated, single drumlins of the LGM maximum phase remain in the Untersee lobe; nevertheless, some hints of ice flow geometry can be gained from the shape of the Schaffhausen frontal moraines. A marked moraine re-entrant between the Schussen and Untersee lobes (Figure 3) suggests that the Höchstlen topographic high (maximum elevation of 838 m a.s.l.) presented a major impediment to ice flow. Frontal moraines at the re-entrant reach ~760 m a.s.l. Further to the west, at Hohenstoffeln (842 m a.s.l.), in the westernmost sector of the Untersee lobe, the ice margin wrapped around the volcanic neck on the west and east (Figures 3 and 11a). Frontal moraines along the southeast slope of Hohenstoffeln give an elevation of 660 m a.s.l. for the front of the ice.

Basal flow directions derived from the fs SHmax b bedforms of the Thur lobe near Andelfingen show west-northwest flow (Figure 9). This agrees well with the modelled directions for the downstream parts of Thur Valley (Cohen et al., 2018). LGM maximum ice is interpreted to have covered nearby Schienerberg (716 m a.s.l.; Figure 3) and Stammerberg (640 m a.s.l.) (Hofmann, 1973; Zaugg & Geyer, 2008) giving minimum ice surface elevations during the Schaffhausen stadial (Figure 11a).

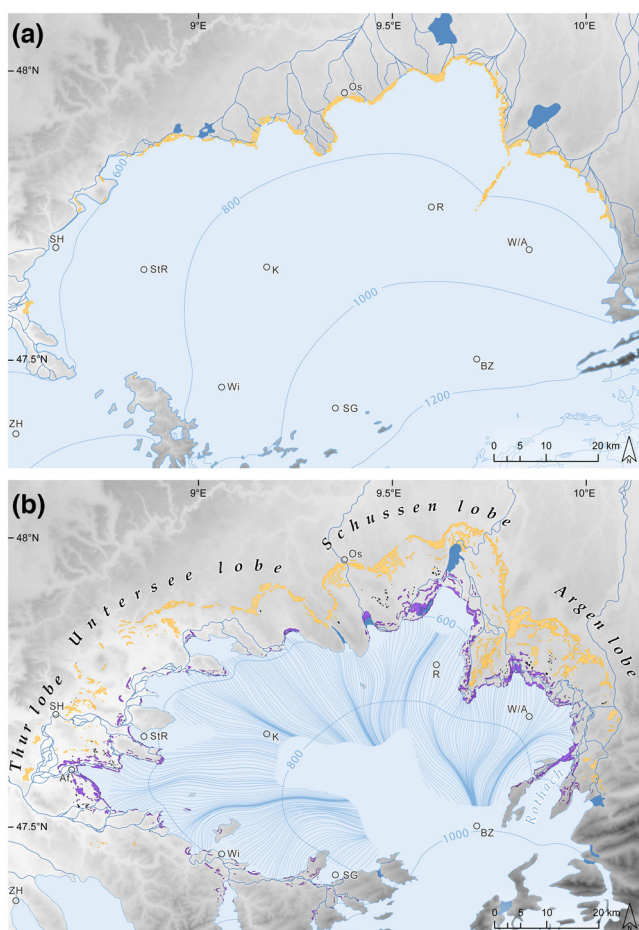


**FIGURE 11** Evolution of the Last Glacial Maximum (LGM) Rhine glacier on the northern Alpine foreland: (a) LGM maximum (modified after Bini et al., 2009). (b) Late LGM readvance to Stein am Rhein ice margin with basal flow lines reconstructed on the basis of subglacial landform orientations (drumlins and glacial lineations) clipped to the 15° kriging standard deviation contour (Section 3.3 and Figure S2) and to the reconstructed extent of the Stein am Rhein stadial glacier. Glacier reconstruction and ice surface elevations based on mapped moraine ridges; glacier extents and ice levels in the northern Alpine mountain ranges modified after Keller and Krays (2005). [Color figure can be viewed at [wileyonlinelibrary.com](http://wileyonlinelibrary.com)]

The southwest basal flow of fs SHmax a drumlins points to ice that very much followed the valleys. This is in contrast to numerical modelling results of Cohen et al. (2018), where a dominance of north-west flow was found for that area.

Along the southern flank of the piedmont lobe, the configuration becomes more complicated due to ice coming in from the south. Ice masses from Toggenburg flowed northwards onto the foreland to meet the Rhine glacier near the town of Wil (Figures 3 and 11a). Ice that filled the lower Alpenrhein Valley up to 1200–1400 m a.s.l. (Bini et al., 2009; Eugster et al., 1960; Hantke, 2003; Hofmann, 1973; Jäckli, 1962; Keller, 1981; Keller & Krayss, 1980, 2005) poured over and across Appenzell, reaching the foreland near St. Gallen. Coalescence of ice masses from both Toggenburg and Appenzell is evidenced by the lack of LGM maximum (Schaffhausen stadial) moraines all along the southern sector (Bini et al., 2009; Hofmann, 1993; Hottinger et al., 1970; Jäckli, 1962; Kamleitner et al., 2023; Keller, 1981).

The isolated bedrock highs (Figures 3 and 11) of Imebärg (707 m a.s.l.), Nollen (735 m a.s.l.) and Ätschberg (906 m a.s.l.) were completely covered by ice during the Schaffhausen stadial (Hofmann, 1973; Zaugg & Geyer, 2008). But we did not observe streamlined landforms on their tops. We interpret these highs to have been under areas of 'passive ice' as discussed, for example, by Punkari (1997, 1980) for the LGM Scandinavian ice sheet. Numerical simulations suggest that ice on the bedrock highs within the lobes may have been cold-based due to transference of cold atmospheric temperatures through thin ice to the glacier base (Cohen, 2017), hindering drumlin formation due to stagnant or sluggish ice patches. Notably, several of these foreland highs (Höchsten, Schienerberg, Stammerberg and Ätschberg; Figure 3) retain remnant Deckenschotter deposits (Early to Middle Pleistocene glaciofluvial gravels; Ellwanger et al., 2011; Graf, 2009; Graf & Burkhalter, 2016; Preusser et al., 2011). Even over several glacial cycles, modification by overriding ice was apparently limited.

The near-complete lack of drumlins in the areas between the Schaffhausen and Stein am Rhein ice margins (Figure 3) has puzzled geologists for decades (Habbe, 1988, 1989). Drumlins of the maximum flow subsets (fs SHmax a–d) occur several kilometres upstream from the LGM maximum paleoglacial front (Figure 9). This implies that the minimum ice thickness was sufficient for the ice to flow and create subglacial streamlined landforms. An ice thickness greater than ~100 m can be estimated (cf. Colgan & Mickelson, 1997; Iverson et al., 2017; Krüger & Thomsen, 1984; Patterson & Hooke, 1995), also in agreement with the geomorphological evidence for ice surface height discussed above. Along the margin itself, a stagnating, low-flow situation near the front of the glacier may have inhibited drumlin formation. Evidence of permafrost in ice-free areas north of the Alps is abundant (Frenzel et al., 1992; Lindgren et al., 2016; Vandenberghe et al., 2014). Cold-based ice at the fringes of the LGM Rhine glacier ice margin has been suggested (Blatter & Haeberli, 1984; Cohen, 2017; Cohen et al., 2018; Haeberli et al., 1984; Haeberli & Penz, 1985), which could as well explain the missing drumlins (Ellwanger, 1992; Habbe, 1989, 1992; Menzies & Habbe, 1992; Menzies & Maltman, 1992). The absence of drumlins may also be a question of lack of preservation rather than lack of formation, especially in the low-lying areas. The frequently observed dissection of glacial landforms especially of the inner Schaffhausen stadial moraines points to vigorous erosion by meltwater, particularly at the fronts of

the Thur and Untersee lobes. Much of the meltwater was routed parallel to but internal to the terminal moraines when the glacier lay slightly behind its maximum position (Keller & Krayss, 2000). If not obliterated by meltwater, outwash deposition could have drowned the drumlins. The reversed drainage situation (back towards the former tongue area; Figure 11b), particularly in the central and eastern sectors, led to the formation of proglacial lakes (Keller & Krayss, 2000, 2005); lake and delta deposits may have buried subglacial landforms.

## 5.2 | The Rhine glacier during the Stein am Rhein stadial

Following a prolonged stillstand at the outer Schaffhausen stadial moraines (Kamleitner et al., 2023; Preusser et al., 2007), Rhine glacier underwent stepwise retreat. Subparallel moraine ridges, of which today only fragments remain (Figure 3) (Kamleitner et al., 2023; Keller & Krayss, 2005), were left behind. Inboard of the Schaffhausen ice marginal complex and often related to outwash plains, hummocky terrain formed in ice decay areas. The oscillating glacier retreated back some tens of kilometres to a position closer to the area of present-day Lake Constance and then underwent readvance (Ellwanger et al., 2011; Heinz, 2001; Keller & Krayss, 2005; Schindler et al., 1978; Schreiner, 1992b). During readvance, the continuous, stacked moraine chains of the Stein am Rhein stadial were built (after 21 ka; Kamleitner et al., 2023). Subglacially streamlined bedforms of flowset fs StR formed during this readvance. Building on the observational data from the drumlins and glacial lineations, our kriging results for flowset fs StR provide an up-close look at basal flow of the Rhine glacier during the Stein am Rhein stadial (Figures 10 and 11b).

In the kriged basal flow patterns (Figure 10) of the central Argen lobe, a divergence of flow orientations north of Lindau is particularly evident. North-flowing ice split into northwest and northeast components. This area is characterized by drumlinized subglacial ribs (Figure 4d), the only occurrence of this type of subglacial landform on the Rhine foreland. The ribs stretch along a west–east axis, that is, perpendicular to the reconstructed basal flow direction. Subglacial ribs have been interpreted as landforms formed under slower stagnating ice flow (Barchyn et al., 2016; Dunlop & Clark, 2006; Stokes, 2018; Stokes et al., 2007) and may develop in areas of compressional flow at the transition from fast- to slow-flowing zones (Stokes et al., 2008). The presence of approximately 100 to 150 m of glacial and related sediments (Grünvogel, 1953; Habicht et al., 1986; Regierungspräsidium Freiburg Landesamt für Geologie, 2013; Schmidt & Müntz, 1979; Schreiner, 1976) may have played a role in their deformation into transverse ridges as discussed by Stokes (2018). Another indication of relatively slower ice may be the presence of near-circular drumlins superimposed on the subglacial ribs. Formation of ribs and drumlins is thought to occur in close succession (Clark & Meehan, 2001). Recent modelling by Ely et al. (2023) supports the concept that subglacial ribs may provide an initiation point for drumlin formation. Due to reorganization of flow, low basal velocities at the Argen ice divide that separates fast-flowing streams to the northwest (Schussen Valley) and northeast (Leiblach Valley) are suggested (Figure 10).

Along Leiblach Valley, faster basal flow is indicated by the marked elongation of the drumlins and the presence of long glacial lineations

(Figure 6). The Leiblach fast-flow corridor coincides with a 20- to 40-m overdeepened trough (Ellwanger et al., 2011; GeoMol Team, 2015). The trough may have already been filled with sediment at the time of bedform formation as suggested by the lack of offset in surface elevation between neighbouring drumlins in and beyond the narrow trough (Figure 6). The presence of easily deformable glaciolacustrine deposits (Regierungspräsidium Freiburg Landesamt für Geologie, 2013; Schmidt & Bräuhäuser, 1985) may have promoted fast basal ice flow. Glacier flow numerical model results as well depict fast ice flow in Leiblach Valley (Cohen et al., 2018; Imhof et al., 2019).

During the Stein am Rhein stadial, a new interlobate complex ( $\sim 8 \text{ km}^2$ ,  $\sim 10 \text{ km}$  long and up to  $1.5 \text{ km}$  wide) developed between the Argen lobe and the newly independent Rothach tributary lobe (Figure 11b). Ice divided south of Pfänder ridge (maximum elevation of  $1069 \text{ m a.s.l.}$ ; Figure 3), flowed northeast along Leiblach and Rothach valleys and then rejoined a few kilometres downstream. At the join, flow from both lobes was towards the suture, as also interpreted for interlobate areas of the Laurentide Ice Sheet (e.g., Oak Ridges moraine; Sookhan et al., 2018) and the Scandinavian Ice Sheet (Punkari, 1997). This flow pattern is in good agreement with our kriged flow trajectories for the easternmost part of the Argen lobe, although based on a small number of observations (Figure 10).

The height of the ice surface along the right side of the Argen lobe can be estimated from the elevations of the Argen–Rothach interlobate ridges (reaching up to  $860 \text{ m a.s.l.}$  on the upstream end of the suture zone and dropping down to  $710 \text{ m a.s.l.}$  at the frontal moraines). Comparing this to elevations of nearby streamlined bedforms, which mark the base of the former Rhine glacier at the foot of Pfänder ridge, an ice thickness of approximately  $350 \text{ m}$  can be reconstructed for the southwestern part of the Argen lobe.

By the Stein am Rhein stadial, the interlobate suture between the Argen and Schussen lobes had evolved into a moraine re-entrant (Figure 11b). Ice levels there were in the range of  $670\text{--}700 \text{ m a.s.l.}$  Kriging results portray ice flowing to the north and northnortheast for the Schussen lobe (Figure 10) and indicate that ice was initially strongly channelized by the Lake Constance basin (northwest flow) and then flowed northwards into the Schussen trough (Figure 6) (Ellwanger et al., 2011; Heuberger et al., 2012; Jordan, 2010; Pietsch & Jordan, 2014; Schnellmann et al., 2014). Highly elongated drumlins and multiple long glacial lineations in the central part of the Schussen drumlin field point to fast-flowing ice near the bottom of Schussen Valley (Figure 6). This was seen as well in numerical modelling results (Cohen et al., 2018; Imhof et al., 2019). Ice flow was rigorously funneled in the Schussen overdeepened trough as no signs of splaying are observed. In contrast, the basal flow pattern on the elevated Molasse ramp just to the west of Schussen Valley shows that flow diverged a bit towards the glacier margin. In the very west of the Schussen lobe, at the point of contact between Schussen and Linzer Aach valleys, Gehrenberg ( $754 \text{ m a.s.l.}$ ) seems to have presented an obstacle to the here about  $300\text{-m}$ -thick, expanding glacier. Ice flowing out of Lake Constance basin diverged south of Gehrenberg and was partly deflected to the left and right of the mountain's base. Downstream, the conspicuous ice front re-entrant along Hächsten topographic high that had already separated Schussen and Untersee lobes during the LGM maximum (Schaffhausen stadial) opened up further during Stein am Rhein stadial (Figure 11b). This is evident from frontal moraine deposits in the valleys to the east and west of Hächsten.

Along the steep slopes of the plateau itself, ice marginal deposits (Figure 3) yield a minimum ice surface level of  $\sim 680 \text{ m a.s.l.}$

At the Untersee lobe, the kriged patterns point to basal ice flow following the SE–NW oriented axis of the Lake Constance basin (Figure 10). Further downglacier, flow was focused along the overdeepened Linzer Aach Valley and the narrow troughs of Zellersee and Überlingersee (Figure 6) (Ellwanger et al., 2011; GeoMol Team, 2015). Westnorthwest and northnorthwest flow trajectories dominate on the western and eastern margins of the Bodanrück peninsula, respectively, as ice deviated around the Molasse bedrock high. At its northern end, the ice surface reached  $\sim 600 \text{ m a.s.l.}$  as suggested by the frontal moraines. While not as clear as in the eastern and western parts of the Rhine foreland, Zellersee and Überlingersee may have hosted faster flowing ice. This assumption is based on slightly higher drumlin L:W ratios at the margins of the Bodanrück peninsula and the southwestern parts of the Linzgau drumlin field where a number of long glacial lineations occur. High sliding speeds were modelled for ice in the Lake Constance basin, as at Zellersee and Überlingersee (Cohen et al., 2018; Imhof et al., 2019).

Kriging results point to dominant westward flow in the central part of the narrow Thur Valley (Figure 10). Here, bedform elongations are high (Figure 6), indicating fast-flowing ice along the overdeepened trough (Jordan, 2010; Pietsch & Jordan, 2014) in agreement with modelled high sliding speeds (Cohen et al., 2018). Moraines along the eastern end of Stammerberg indicate a maximum ice surface height near the ice margin of  $\sim 650 \text{ m a.s.l.}$  South of Stammerberg, on the right side of Thur Valley, drumlins are found as low as  $\sim 420 \text{ m a.s.l.}$ , suggesting about  $230 \text{ m}$  of overlying ice.

The eastern parts of the Oberthurgau drumlin field (Figure 5) are dominated by ice flowing to the west out of the Lake Constance basin (Figure 10). In the western part of the Oberthurgau drumlin field, ice flow was concentrated in a valley between the Imebärg and Nollen highs. Potentially maintaining higher basal velocities, Oberthurgau ice flow turned towards the southwest in the direction of Hörnli mountain. In accordance with the observations from the subglacial record, a modelling study by Imhof et al. (2019) consistently predicts fast flow in the area of Oberthurgau. Closer to the Stein am Rhein frontal moraines, splaying flow under relatively slower velocities is suggested by diverging drumlin directions and decrease of L:W ratios. Ice levels at around  $700 \text{ m a.s.l.}$  are indicated by lateral moraines on the southern part of Imebärg. Local ice thickness must have been around  $230 \text{ m}$ . The highest parts of Imebärg and Nollen likely protruded from the ice as nunataks (cf. Hofmann, 1973).

In the Fürstenland field (Figure 5), a distinctive leftward turn in basal ice flow is depicted by the kriging results (Figure 10). Ice initially flowing due west conspicuously curves around the base of Ätschberg mountain to flow towards the southsouthwest, eventually to point due south. Ätschberg was by the Stein am Rhein stadial a nunatak (Figures 3 and 11b; Keller & Krays, 2005). The ice surface was no higher than  $800 \text{ m a.s.l.}$  as defined by the moraines along Ätschberg's western side. Accordingly, the Fürstenland drumlin field was likely covered by around  $230 \text{ m}$  of ice. Ice flowing around the base of Ätschberg did not rejoin on the downstream side of the mountain. Instead, an individual glacier tongue terminated at the frontal moraine ridges west of St. Gallen (Figure 11b).

By the time of the Stein am Rhein stadial, the southern tributary glaciers no longer reached the Swiss foreland (Figure 11b). This is

clearly shown by the strings of frontal moraines built by south-flowing ice of the Rhine piedmont lobe (Figure 3) (Hottinger et al., 1970; Kamleitner et al., 2023; Keller & Krayss, 1980, 2005). Drumlins that exhibit clear splaying terminate at this moraine set. The front of the ice coming out of Toggenburg was located in an upstream position (Keller, 1981; Keller & Krayss, 1980, 2000, 2005), as evidenced by frontal moraines 5 km south of Wil (Keller & Krayss, 2005). Due to lowered ice surface heights in Alpenrhein Valley – Keller and Krayss (2005) estimated ice surface heights of 1200–1000 m a.s.l. – by the Stein am Rhein stadial, little ice overspilled into the Appenzell region (Figures 1 and 11b). Mapped frontal moraines south and southeast of St. Gallen (Keller & Krayss, 2005; Figure 3) record north-flowing ice from accumulation areas of Alpstein massif (Figures 1 and 11b). The observed drumlin orientations in the Fürstentland and Oberthurgau fields show that ice was coming out of the Lake Constance basin and flowing to the southwest and south, actually back towards the mountains (Figure 10). If substantial ice masses had crossed over Appenzell from the Alpenrhein Valley, the marked southwest and southward basal flow patterns would not have been possible.

### 5.3 | Comparison of Schaffhausen and Stein am Rhein stadial ice flow geometries

The Rhine glacier ice surface during the Schaffhausen stadial descended smoothly from 1200 m a.s.l. at the mouth of the Alpenrhein Valley to the frontal moraines at 770 m a.s.l. in the easternmost sector and as low as 430 m a.s.l. in the very western sector (Bini et al., 2009; Jäckli, 1962; Kamleitner et al., 2023; Keller & Krayss, 2005). Ice thickness was likely highly variable, thickening in the overdeepened basins and troughs (Figure 6) and thinning on higher parts of the topography (Figure 1c). Estimating ice thickness is further hampered by the limited knowledge on the ages of basin infills (cf. Ellwanger et al., 2011; Fabbri et al., 2021; GeoMol Team, 2015; Jordan, 2010; Schaller et al., 2022; Wessels et al., 2015). The formerly broad and nearly equant Rhine piedmont lobe of Schaffhausen stadial (Figure 11a) upon readvance (Stein am Rhein stadial) presented individual lobes more strongly confined by the existing troughs (Figures 6 and 11b). The presence of corridors of fast-flowing ice in the existing troughs is not readily apparent in the shape of the vigorous Schaffhausen stadial piedmont lobe. Nevertheless, hints are given at in the shape of the frontal moraines where they protrude beyond their neighbours, for example, at the Schussen lobe. The Schaffhausen stadial lobe configuration is especially marked in the eastern sector where the Argenschussen suture built up (cross-section given in Kamleitner et al., 2023). During the Stein am Rhein readvance, the ice surface was about 200 m lower, the ice thickness consequently less. Where revealed by geomorphological evidence, ice thickness above drumlin fields was found to range from about 350–230 m and was thus relatively thin. This fostered the marked topographic control on ice flow that is clearly depicted in the streamlined subglacial bedforms and the derived flow lines (Figure 10). The distinct lack of overprinting of generations of subglacial bedforms suggests that either few bedforms evolved during the Schaffhausen stadial or they were completely remoulded during the Stein am Rhein readvance. Even close to the Stein am Rhein ice margin, the local splaying depicted by

the bedforms does not reveal any smudging. This suggests that the observed bedforms internal to the Stein am Rhein ice margin formed very late in the readvance phase, under stable ice flow by an active partially warm-based polythermal glacier. From a subglacial point of view, any minor recessional stadial (Konstanz; Keller & Krayss, 2005) was likely only a brief halt during retreat and had no apparent impact on the streamlined subglacial landforms. Glacier disintegration from the Alpine foreland was likely fast and continuous as shown by the distinct imprint of bedforms, the absence of progressive upstream fanning of drumlin orientations, and the near-complete lack of stabilization moraines or ice decay deposits (cf. Evans & Twigg, 2002; Szuman et al., 2021).

## 6 | CONCLUSIONS

The footprint of the LGM Rhine glacier in the northeastern Swiss and southwestern German Alpine forelands yields a rich glacial geomorphological record. On the basis of high-resolution elevation data, we mapped ice marginal moraines and more than 2500 subglacially streamlined landforms. For the first time, a consistent (digital) inventory of streamlined bedforms is available covering the entire LGM Rhine glacier piedmont lobe. The dataset comprises predominantly drumlins and also includes glacial lineations and subglacial ribs. Mapped streamlined subglacial bedforms comprise two distinct flowsets as evidenced by morphological criteria, proximity and parallel conformity: the Schaffhausen flowset and the Stein am Rhein flowset.

Directional information from the Schaffhausen flowset (equivalent to the LGM maximum phase = Schaffhausen stadial) is visually generalized, revealing topographically controlled ice flow near the LGM maximum glacier margins.

The Stein am Rhein flowset holds more than 2400 drumlins and glacial lineations, all located upstream of the Stein am Rhein ice margin. Based on consistency of morphometries and local orientations, we assess this as an isochronous flowset, formed during the late LGM glacier readvance to and the active stabilization at the Stein am Rhein ice margin. The splaying pattern of drumlins that occurs all along and just upstream of the Stein am Rhein ice margin demonstrates that landforms of the Stein am Rhein flowset are unrelated to the outboard drumlins of the Schaffhausen flowset. The absence of overlapping fan pattern of younger generations of subglacially streamlined bedforms upstream and the lack of evidence of remoulding further show that downwasting of the Rhine glacier from the foreland was likely rapid and uninterrupted by marked halts.

Using a recently presented kriging approach (Ng & Hughes, 2019), we interpolated the orientations of the Stein am Rhein flowset to create a basal ice flow surface. Results yield objective 2D flow reconstructions of the late LGM Rhine glacier foreland lobe and display a radial basal ice flow, emanating from the basin of Lake Constance and fanning out to the margins in southwestern, western, northwestern, northern and northeastern directions. Driven by topographic constraints, the basal flow pattern shows zones of converging and diverging ice flow under shallow ice. Geomorphologically constrained ice thicknesses over the drumlin fields were approximately 350–230 m. Gained flow lines combined with information on bedform elongation delineate potential areas of high basal velocities. Suggested corridors of fast-flowing ice are located in Oberthurgau, Thur Valley,

Schussen Valley, Leiblach Valley, and less distinctly implied parallel to Lake Constance and Überlingersee. Geomorphologically reconstructed zones of potentially higher basal velocity largely coincide with known overdeepenings.

Streamlined subglacial landforms hold unique information on basal flow directions and relative basal flow velocity differences of long vanished ice masses. Combining the linear information from bedform orientation to flow fields, visually or by means of kriging (Ng & Hughes, 2019), is an elegant tool to reconstruct laminar paleo-ice flow patterns. So far mainly applied in the context of the Northern Hemispheric ice sheets, we show that information inferred from streamlined bedforms equally complements our understanding of glacier dynamics on the Alpine forelands and provides explicit physical evidence to validate future numerical modelling studies.

## AUTHOR CONTRIBUTIONS

**Sarah Kamleitner:** Conceptualization; methodology; investigation; resources; writing—initial draft; writing—reviewing and editing; figure design. **Susan Ivy-Ochs:** Conceptualization; funding acquisition; investigation; writing—initial draft; writing—reviewing and editing. **Bernhard Salcher:** Investigation; resources; writing—reviewing and editing. **Jürgen M. Reitner:** Investigation; writing—reviewing and editing.

## ACKNOWLEDGEMENTS

We thank editor S. Lane, the associate editor, and the reviewers M. Buechi and W. Haeberli for insightful review and valuable comments. We acknowledge Felix Ng and Anna Hughes for answering our queries on the implementation of the MATLAB code. The help of Paul Ochs in optimizing our curve-fitting routine is greatly appreciated. Urs H. Fischer and Denis Cohen are thanked for providing insights into glacier dynamics and modelling and for discussing their recent LGM Rhine glacier model results. Further, we thank the Swiss Federal Office of Topography for supplying high-resolution DEMs and appreciate the granted discount on elevation data by the Bavarian Agency for Digitization, High-Speed Internet and Surveying. Funding for this research was provided by the Swiss National Science Foundation (Schweizerischer Nationalfonds zur Förderung der Wissenschaftlichen Forschung [SNF] Grant Number 175794, 2017).

## DATA AVAILABILITY STATEMENT

Data are available upon reasonable request.

## ORCID

Sarah Kamleitner  <https://orcid.org/0000-0002-5951-9793>

Susan Ivy-Ochs  <https://orcid.org/0000-0002-3242-9536>

Bernhard Salcher  <https://orcid.org/0000-0002-1061-6090>

Jürgen M. Reitner  <https://orcid.org/0000-0001-6190-6736>

## REFERENCES

- Barchyn, T.E., Dowling, T.P.F., Stokes, C.R. & Hugenholtz, C.H. (2016) Subglacial bed form morphology controlled by ice speed and sediment thickness. *Geophysical Research Letters*, 43(14), 7572–7580. Available from: <https://doi.org/10.1002/2016GL069558>
- Beckenbach, E., Müller, T., Seyfried, H. & Simon, T. (2014) Potential of a high-resolution DTM with large spatial coverage for visualization, identification and interpretation of young (Würmian) glacial geomorphology: a case study from Oberschwaben (southern Germany). *E&G Quaternary Science Journal*, 63(2), 107–129. Available from: <https://doi.org/10.3285/eg.63.2.01>
- Bennett, M.R. & Glasser, N.F. (2009) *Glacial geology: ice sheets and landforms*. Chichester: Wiley-Blackwell.
- Benz-Meier, C. (2003) Der würmezeitliche Rheingletscher—Maximalstand Digitale Rekonstruktion, Modellierung und Analyse mit einem Geographischen Informationssystem. PhD thesis, Universität Zürich.
- Bini, A., Buoncristiani, J.-F., Couterrand, S., Ellwanger, D., Felber, M., Florineth, D., et al. (2009) *Die Schweiz während des letzteiszeitlichen Maximums (LGM)*. Wabern: Bundesamt für Landestopografie swisstopo.
- Blatter, H. & Haeberli, W. (1984) Modelling temperature distribution in Alpine glaciers. *Annals of Glaciology*, 5, 18–22. Available from: <https://doi.org/10.3189/1984AoG5-1-18-22>
- Bodenburg Hellmund, H.W. (1909) Die Drumlinlandschaft zwischen Pfäffiker- und Greifensee. *Vierteljahrsschrift der Naturforschenden Gesellschaft in Zürich*, 54, 149–216.
- Boulton, G.S. (1987) A theory of drumlin formation by subglacial sediment deformation. In: Menzies, J. & Rose, J. (Eds.) *Drumlin symposium*. Rotterdam: Balkema, pp. 25–80.
- Boulton, G.S. & Clark, C.D. (1990a) The Laurentide ice sheet through the last glacial cycle: the topology of drift lineations as a key to the dynamic behaviour of former ice sheets. *Transactions of the Royal Society of Edinburgh: Earth Sciences*, 81(4), 327–347. Available from: <https://doi.org/10.1017/S0263593300020836>
- Boulton, G.S. & Clark, C.D. (1990b) A highly mobile Laurentide ice sheet revealed by satellite images of glacial lineations. *Nature*, 346(6287), 813–817. Available from: <https://doi.org/10.1038/346813a0>
- Boyes, B.M., Pearce, D.M. & Linch, L.D. (2021) Glacial geomorphology of the Kola Peninsula and Russian Lapland. *Journal of Maps*, 17(2), 485–503. Available from: <https://doi.org/10.1080/17445647.2021.1970036>
- Brauhäuser, M. (1976) *Erläuterungen zu Blatt 8322 Friedrichshafen. Geologische Karte von Baden-Württemberg 1:25 000*. Stuttgart: Geologisches Landesamt Baden-Württemberg.
- Brückner, E. (1886) Die Vergletscherung des Salzachgebietes. In: *Geographische Abhandlungen*. Wien: Ed. Hölzel.
- Buechi, M.W., Frank, S.M., Graf, H.R., Menzies, J. & Anselmetti, F.S. (2017) Subglacial emplacement of tills and meltwater deposits at the base of overdeepened bedrock troughs. *Sedimentology*, 64(3), 658–685. Available from: <https://doi.org/10.1111/SED.12319>
- Carlson, A.E., Mickelson, D.M., Principato, S.M. & Chapel, D.M. (2005) The genesis of the northern Kettle Moraine, Wisconsin. *Geomorphology*, 67(3–4), 365–374. Available from: <https://doi.org/10.1016/j.geomorph.2004.11.003>
- Chandler, B.M.P., Lovell, H., Boston, C.M., Lukas, S., Barr, I.D., Benediktsson, Í.Ö., et al. (2018) Glacial geomorphological mapping: a review of approaches and frameworks for best practice. *Earth-Science Reviews*, 185, 806–846. Available from: <https://doi.org/10.1016/j.earscirev.2018.07.015>
- Clark, C.D. (1993) Mega-scale glacial lineations and cross-cutting ice-flow landforms. *Earth Surface Processes and Landforms*, 18(1), 1–29. Available from: <https://doi.org/10.1002/esp.3290180102>
- Clark, C.D. (1994) Large-scale ice-moulding: a discussion of genesis and glaciological significance. *Sedimentary Geology*, 91(1–4), 253–268. Available from: [https://doi.org/10.1016/0037-0738\(94\)90133-3](https://doi.org/10.1016/0037-0738(94)90133-3)
- Clark, C.D. (1999) Glaciodynamic context of subglacial bedform generation and preservation. *Annals of Glaciology*, 28, 23–32. Available from: <https://doi.org/10.3189/172756499781821832>
- Clark, C.D. (2010) Emergent drumlins and their clones: from till dilatancy to flow instabilities. *Journal of Glaciology*, 51(200), 1011–1025. Available from: <https://doi.org/10.3189/002214311796406068>
- Clark, C.D., Ely, J.C., Greenwood, S.L., Hughes, A.L.C., Meehan, R., Barr, I.D., et al. (2018) BRITICE Glacial Map, version 2: a map and GIS database of glacial landforms of the last British–Irish Ice Sheet. *Boreas*, 47, 11–27. Available from: <https://doi.org/10.1111/bor.12273>
- Clark, C.D., Ely, J.C., Spagnolo, M., Hahn, U., Hughes, A.L.C. & Stokes, C.R. (2018) Spatial organization of drumlins. *Earth Surface Processes and*

- Landforms*, 43(2), 499–513. Available from: <https://doi.org/10.1002/esp.4192>
- Clark, C.D., Hughes, A.L.C., Greenwood, S.L., Spagnolo, M. & Ng, F.S.L. (2009) Size and shape characteristics of drumlins, derived from a large sample, and associated scaling laws. *Quaternary Science Reviews*, 28(7–8), 677–692. Available from: <https://doi.org/10.1016/j.quascirev.2008.08.035>
- Clark, C.D., Knight, J.K. & Gray, J.T. (2000) Geomorphological reconstruction of the Labrador sector of the Laurentide Ice Sheet. *Quaternary Science Reviews*, 19(13), 1343–1366. Available from: [https://doi.org/10.1016/S0277-3791\(99\)00098-0](https://doi.org/10.1016/S0277-3791(99)00098-0)
- Clark, C.D. & Meehan, R.T. (2001) Subglacial bedform geomorphology of the Irish Ice Sheet reveals major configuration changes during growth and decay. *Journal of Quaternary Science*, 16(5), 483–496. Available from: <https://doi.org/10.1002/JQS.627>
- Clark, C.D., Tulaczyk, S.M., Stokes, C.R. & Canals, M. (2003) A groove-ploughing theory for the production of mega-scale glacial lineations, and implications for ice-stream mechanics. *Journal of Glaciology*, 49(165), 240–256. Available from: <https://doi.org/10.3189/172756503781830719>
- Cohen, D. (2017) *Arbeitsbericht NAB 17-25. Numerical reconstruction of the Rhine Glacier at the Last Glacial Maximum*. Wettingen: Nagra.
- Cohen, D., Gillet-Chaulet, F., Haeberli, W., Machguth, H. & Fischer, U.H. (2018) Numerical reconstructions of the flow and basal conditions of the Rhine glacier, European Central Alps, at the Last Glacial Maximum. *The Cryosphere*, 12(8), 2515–2544. Available from: <https://doi.org/10.5194/tc-12-2515-2018>
- Colgan, P.M. & Mickelson, D.M. (1997) Genesis of streamlined landforms and flow history of the Green Bay Lobe, Wisconsin, USA. *Sedimentary Geology*, 111(1–4), 7–25. Available from: [https://doi.org/10.1016/S0037-0738\(97\)00003-1](https://doi.org/10.1016/S0037-0738(97)00003-1)
- Custer, W. & Aubert, D. (1935) *Cossonay. Atlas géologique de la Suisse 1: 25 000 no. 5*. Zürich: J.C. Müller.
- de Jong, M.G.G. (1983) *Quaternary deposits and landforms of western Allgäu (Germany) and the deglaciation after the last major Pleistocene ice advance*, Vol. 36. Amsterdam: Fysisch Geografisch en Bodemkundig Laboratorium Universiteit van Amsterdam.
- Dunlop, P. & Clark, C.D. (2006) The morphological characteristics of ribbed moraine. *Quaternary Science Reviews*, 25(13–14), 1668–1691. Available from: <https://doi.org/10.1016/j.quascirev.2006.01.002>
- Dunlop, P., Clark, C.D. & Hindmarsh, R.C.A. (2008) Bed ribbing instability explanation: testing a numerical model of ribbed moraine formation arising from coupled flow of ice and subglacial sediment. *Journal of Geophysical Research—Earth Surface*, 113(F3), 1–15, F03005. Available from: <https://doi.org/10.1029/2007JF000954>
- Ebers, E. (1926) Das Eberfinger Drumlinfeld. Geologisch-morphologische Studie. In: *Geologische Landesuntersuchung*. (Ed.) *Geognostische Jahreshefte*. München: Piloty & Loehle, pp. 47–86.
- Ebers, E. (1960) Drumlinkerne, ältere Würmschotter und das Würm-Interstadial-Profil von Hörmating/Obb. *E&G Quaternary Science Journal*, 11(1), 64–76. Available from: <https://doi.org/10.3285/EG.11.1.08>
- Ehlers, J., Gibbard, P.L. & Hughes, P.D. (2011) *Quaternary glaciations—extent and chronology. A closer look*. Amsterdam: Elsevier.
- Ellwanger, D. (1990) Würmzeitliche Drumlinformung bei Markelfingen (westlicher Bodensee, Baden-Württemberg). *Jahresberichte und Mitteilungen des Oberrheinischen Geologischen Vereins*, 72, 411–434. Available from: <https://doi.org/10.1127/jmogv/72/1990/411>
- Ellwanger, D. (1992) Lithology and stratigraphy of some Rhine glacier drumlins (South German Alpine Foreland). *Geomorphology*, 6(1), 79–88. Available from: [https://doi.org/10.1016/0169-555X\(92\)90050-X](https://doi.org/10.1016/0169-555X(92)90050-X)
- Ellwanger, D. (1994) Observations on drumlinized till in the Rhine glacier area (South German Alpine foreland). In: Warren, W.P. & Croot, D.G. (Eds.) *Formation and deformation of glacial deposits*. Rotterdam: A. A. Balkema, pp. 115–125.
- Ellwanger, D., Wielandt-Schuster, U., Franz, M. & Simon, T. (2011) The Quaternary of the southwest German Alpine Foreland (Bodensee-Oberschwaben, Baden-Württemberg, Southwest Germany). *E&G Quaternary Science Journal*, 60(2/3), 306–328. Available from: <https://doi.org/10.3285/eg.60.2-3.07>
- Ely, J.C., Stevens, D., Clark, C.D. & Butcher, F.E.G. (2023) Numerical modelling of subglacial ribs, drumlins, herringbones, and mega-scale glacial lineations reveals their developmental trajectories and transitions. *Earth Surface Processes and Landforms*, 48(5), 1–23. Available from: <https://doi.org/10.1002/esp.5529>
- Erb, L. (1986) Erläuterungen zu Blatt 8221 Überlingen-Ost (früher Mainau). In: *Geologische Karte von Baden-Württemberg 1:25 000*. Stuttgart: Landesvermessungsamt Baden-Württemberg.
- Eugster, H., Fröhlicher, H. & Saxer, F. (1960) *Geologischer Atlas der Schweiz 1:25 000 Blatt St. Gallen—Appenzell*. Bern: Kümmerly & Frey AG.
- European Environment Agency. (2017) *Copernicus Land Monitoring Service—reference data: EU-DEM*. Copenhagen: European Environment Agency.
- Evans, D.J.A. & Twigg, D.R. (2002) The active temperate glacial landsystem: a model based on Breiðamerkjökull and Fjallsjökull, Iceland. *Quaternary Science Reviews*, 21(20–22), 2143–2177. Available from: [https://doi.org/10.1016/S0277-3791\(02\)00019-7](https://doi.org/10.1016/S0277-3791(02)00019-7)
- Eyles, N., Putkinen, N., Sookhan, S. & Arbelaez-Moreno, L. (2016) Erosional origin of drumlins and megaridges. *Sedimentary Geology*, 338, 2–23. Available from: <https://doi.org/10.1016/j.sedgeo.2016.01.006>
- Fabbri, S.C., Affentranger, C., Krastel, S., Lindhorst, K., Wessels, M., Madritsch, H., et al. (2021) Active faulting in Lake Constance (Austria, Germany, Switzerland) unraveled by multi-vintage reflection seismic data. *Frontiers in Earth Science*, 9, 670532. Available from: <https://doi.org/10.3389/feart.2021.670532>
- Fiebig, M., Ellwanger, D. & Doppler, G. (2011) Pleistocene glaciations of southern Germany. In: Ehlers, J., Gibbard, P.L. & Hughes, P.D. (Eds.) *Quaternary glaciations—extent and chronology. A closer look*. Oxford: Elsevier Inc., pp. 163–173. Available from: <https://doi.org/10.1016/B978-0-444-53447-7.00014-3>
- Fitzsimons, S. & Howarth, J. (2017) Glaciolacustrine processes. In: Menzies, J. & van der Meer, J.J.M. (Eds.) *Past glacial environments*. Amsterdam: Elsevier, pp. 309–334. Available from: <https://doi.org/10.1016/B978-0-08-100524-8.00009-9>
- Florineth, D. & Schlüchter, C. (1998) Reconstructing the Last Glacial Maximum (LGM) ice surface geometry and flowlines in the Central Swiss Alps. *Eclogae Geologicae Helveticae*, 91, 391–407. Available from: <https://doi.org/10.7892/boris.87056>
- Fowler, A.C. (2018) The philosopher in the kitchen: the role of mathematical modelling in explaining drumlin formation. *GFF*, 140(2), 93–105. Available from: <https://doi.org/10.1080/11035897.2018.1444671>
- Fowler, A.C. & Chapwanya, M. (2014) An instability theory for the formation of ribbed moraine, drumlins and mega-scale glacial lineations. *Proceedings of the Royal Society A: Mathematical, Physical and Engineering Sciences*, 470(2171), 20140185. Available from: <https://doi.org/10.1098/RSPA.2014.0185>
- Frenzel, B., Pécsi, M. & Velichko, A.A. (Eds.) (1992) *Atlas of paleoclimates and paleoenvironments of the Northern Hemisphere. Late Pleistocene–Holocene*. Budapest, Stuttgart: Hungarian Academy of Sciences, Gustav Fischer Verlag.
- Früh, J. (1904) Neue Drumlinlandschaft innerhalb des diluvialen Rheingletschers. *Eclogae Geologicae Helveticae*, 8, 213–216.
- Geiger, E. (1943) *Geologischer Atlas der Schweiz 1:25 000 Blätter: 56 Pfyn, 57 Märstetten, 58 Frauenfeld, 59 Bussnang*. Bern: Kümmerly & Frey AG.
- Geiger, E. (1968) *Geologischer Atlas der Schweiz 1:25 000 Blatt 1054 Weinfelden*. Basel: Wassermann AG.
- GeoMol Team. (2015) *GeoMol—assessing subsurface potentials of the Alpine Foreland Basins for sustainable planning and use of natural resources—project report*. Augsburg: Bavarian State Office for Environment.
- German, R. (1977) Zum Problem der Entstehung südböschwäbischer Hügel. *Jahreshefte der Gesellschaft für Naturkunde in Württemberg*, 132, 110–116.
- Glückert, G. (1974) On Pleistocene glaciations in the German Alpine foreland. *Bulletin of the Geological Society of Finland*, 46(2), 117–131. Available from: <https://doi.org/10.17741/bgsf/46.2.004>
- Götzinger, G. (1939) Drumlins und Oser im Traungletschergebiet. *Anzeiger der Akademie der Wissenschaften in Wissenschaften, Mathematische-naturwissenschaftliche Klasse*, 7, 35–39.

- Graf, H.R. (2009) Stratigraphie und Morphogenese von frühpleistozänen Ablagerungen zwischen Bodensee und Klettgau. *E&G Quaternary Science Journal*, 58(1), 12–54. Available from: <https://doi.org/10.3285/eg.58.1.02>
- Graf, H.R. & Burkhalter, R. (2016) Quaternary deposits: concept for a stratigraphic classification and nomenclature—an example from northern Switzerland. *Swiss Journal of Geosciences*, 109(2), 137–147. Available from: <https://doi.org/10.1007/S00015-016-0222-7/FIGURES/5>
- Greenwood, S.L. & Clark, C.D. (2008) Subglacial bedforms of the Irish ice sheet. *Journal of Maps*, 4(1), 332–357. Available from: <https://doi.org/10.4113/jom.2008.1030>
- Greenwood, S.L. & Clark, C.D. (2009) Reconstructing the last Irish Ice Sheet 1: changing flow geometries and ice flow dynamics deciphered from the glacial landform record. *Quaternary Science Reviews*, 28(27–28), 3085–3100. Available from: <https://doi.org/10.1016/J.QUASCIREV.2009.09.008>
- Grünvogel, E. (1953) Über die Drumlins des würmeiszeitlichen Rheingletschers östlich der Schussenschenke. In: *Zum Quartär Der Alpen Und Des Alpenvorlandes*. München: Bayerisches Geologisches Landesamt, pp. 154–163.
- Grünvogel, E. (1954) Stromlinien eines würmeiszeitlichen Rheingletscher-Vorstoßes östlich der Schussenschenke. *Jahreshefte der Gesellschaft für Naturkunde in Württemberg*, 109, 35–46.
- Habbe, K.A. (1988) Zur Genese der Drumlins im süddeutschen Alpenvorland—Bildungsräume, Bildungszeiten, Bildungsbedingungen. *Zeitschrift für Geomorphologie*, 70, 33–50.
- Habbe, K.A. (1989) On the origin of the drumlins of the South German Alpine Foreland. *Sedimentary Geology*, 62(2–4), 357–369. Available from: [https://doi.org/10.1016/0037-0738\(89\)90125-5](https://doi.org/10.1016/0037-0738(89)90125-5)
- Habbe, K.A. (1992) On the origin of the drumlins of the South German Alpine Foreland (II): the sediments underneath. *Geomorphology*, 6(1), 69–78. Available from: [https://doi.org/10.1016/0169-555X\(92\)90049-T](https://doi.org/10.1016/0169-555X(92)90049-T)
- Habicht, H., Müller, G., Schwerd, K., Vuynovich, D. & Zeh, U.M. (1986) *Geologie im östlichen Bodenseegebiet*. Kartenblätter 8423 Kressbronn am Bodensee und 8424 Lindau, Bodensee, Geologica. edition. München: Bayerisches Geologisches Landesamt.
- Haerberli, W. & Penz, U. (1985) An attempt to reconstruct glaciological and climatological characteristics of 18 ka BP Ice Age glaciers in and around the Swiss Alps. *Zeitschrift für Gletscherkunde und Glazialgeologie*, 21, 351–361.
- Haerberli, W., Rellstab, W. & Harrison, W.D. (1984) Geothermal effects of 18 ka BP ice conditions in the Swiss plateau. *Annals of Glaciology*, 5, 56–60. Available from: <https://doi.org/10.3189/1984AoG5-1-56-60>
- Haldimann, P., Graf, H.R. & Jost, J. (2017) *Blatt 1071 Bülach.—Geol. Atlas Schweiz 1:25 000, Karte 151*. Wabern: Bundesamt für Landestopografie swisstopo.
- Hantke, R. (2003) *Blatt 1076 St. Margarethen (Westhälfte) und 1096 Diepoldsau (Westhälfte) mit NW-Ecke von Blatt 1116 Feldkirch.—Geol. Atlas Schweiz 1:25 000, Karte 108*. Bernoulli: Bundesamt für Wasser und Geologie.
- Hart, J.K., Clayton, A.I., Martinez, K. & Robson, B.A. (2018) Erosional and depositional subglacial streamlining processes at Skálafellssjökull, Iceland: an analogue for a new bedform continuum model. *GFF*, 140(2), 153–169. Available from: <https://doi.org/10.1080/11035897.2018.1477830>
- Hättestrand, C., Goodwillie, D. & Kleman, J. (1999) Size distribution of two cross-cutting drumlin systems in northern Sweden: a measure of selective erosion and formation time length. *Annals of Glaciology*, 28, 146–152. Available from: <https://doi.org/10.3189/172756499781821689>
- Heinisch, H., Pestal, G. & Reitner, J.M. (2015) *Erläuterungen zu Blatt 122 Kitzbühel*. Wien: Geologische Bundesanstalt.
- Heinz, J. (2001) Sedimentary geology of glacial and periglacial gravel bodies (SW-Germany). PhD thesis, Universität Tübingen.
- Heuberger, S., Büchi, M. & Naef, H. (2012) *Arbeitsbericht NAB 12-20. Drainage system and landscape evolution of northern Switzerland since the Late Miocene*. Wettingen: Nagra.
- Hillier, J.K., Smith, M.J., Armugam, R., Barr, I., Boston, C.M., Clark, C.D., et al. (2015) Manual mapping of drumlins in synthetic landscapes to assess operator effectiveness. *Journal of Maps*, 11(5), 719–729. Available from: <https://doi.org/10.1080/17445647.2014.957251>
- Hofmann, F. (1967) *Geologischer Atlas der Schweiz 1:25 000 Blatt 1052 Andelfingen*. Bern: Kümmerly & Frey AG.
- Hofmann, F. (1973) *Geologischer Atlas der Schweiz 1:25 000 Blatt 1074 Bischofszell*. Basel: Schweizerische Geologische Kommission.
- Hofmann, F. (1981) *Geologischer Atlas der Schweiz 1:25 000 Blatt: 1031 Neunkirch*. Basel: Schweizerische Geologische Kommission.
- Hofmann, F. (1993) *Geologischer Atlas der Schweiz 1:25 000 Blatt: 1073 Wil*. Bern: Landeshydrologie und -geologie.
- Hofmann, F. (1997) *Blatt 1011 Beggingen (Südhälfte) mit SW-Anteil von Blatt 1012 Singen—Geol. Atlas Schweiz 1:25 000, Karte 97*. Bern: Bundesamt für Wasser und Geologie.
- Hottinger, L., Matter, A., Nabholz, W. & Schindler, C. (1970) *Geologischer Atlas der Schweiz 1:25 000 Blatt: 1093 Hörnli*. Bern: Kümmerly & Frey AG.
- Hübscher, J. (1961) *Geologischer Atlas der Schweiz 1:25 000 Blatt 1032 Diessenhofen mit Anhängsel von Blatt 1031 Neunkirch*. Basel: Wasser-mann AG.
- Hughes, A.L.C., Clark, C.D. & Jordan, C.J. (2010) Subglacial bedforms of the last British Ice Sheet. *Journal of Maps*, 6(1), 543–563. Available from: <https://doi.org/10.4113/jom.2010.1111>
- Hughes, A.L.C., Clark, C.D. & Jordan, C.J. (2014) Flow-pattern evolution of the last British Ice Sheet. *Quaternary Science Reviews*, 89, 148–168. Available from: <https://doi.org/10.1016/J.QUASCIREV.2014.02.002>
- Imhof, M.A., Cohen, D., Seguinot, J., Aschwanden, A., Funk, M. & Jouvét, G. (2019) Modelling a paleo valley glacier network using a hybrid model: an assessment with a Stokes ice flow model. *Journal of Glaciology*, 65(254), 1000–1010. Available from: <https://doi.org/10.1017/jog.2019.77>
- Iverson, N.R., McCracken, R.G., Zoet, L.K., Benediktsson, Í.Ö., Schomacker, A., Johnson, M.D., et al. (2017) A theoretical model of drumlin formation based on observations at Múlajökull, Iceland. *Journal of Geophysical Research—Earth Surface*, 122(12), 2302–2323. Available from: <https://doi.org/10.1002/2017JF004354>
- Ivy-Ochs, S., Monegato, G. & Reitner, J.M. (2022) The Alps: glacial landforms from the Last Glacial Maximum. In: Palacios, D., Hughes, P.D., Ruiz, J.M.G. & de Andrés, N. (Eds.) *European glacial landscapes: maximum extent of glaciations*. Amsterdam: Elsevier, pp. 449–460. Available from: <https://doi.org/10.1016/B978-0-12-823498-3.00030-3>
- Jäckli, H. (1962) Die Vergletscherung der Schweiz im Würmmaximum. *Eclogae Geologicae Helveticae*, 55, 285–294. Available from: <https://doi.org/10.5169/seals-162924>
- Jamieson, S.S.R., Stokes, C.R., Livingstone, S.J., Vieli, A., Cofaigh, C., Hillenbrand, C.D., et al. (2016) Subglacial processes on an Antarctic ice stream bed. 2: can modelled ice dynamics explain the morphology of mega-scale glacial lineations? *Journal of Glaciology*, 62(232), 285–298. Available from: <https://doi.org/10.1017/jog.2016.19>
- Jennings, C.E. (2006) Terrestrial ice streams—a view from the lobe. *Geomorphology*, 75(1–2), 100–124. Available from: <https://doi.org/10.1016/J.GEOMORPH.2005.05.016>
- Jordan, P. (2010) Analysis of overdeepened valleys using the digital elevation model of the bedrock surface of Northern Switzerland. *Swiss Journal of Geosciences*, 103(3), 375–384. Available from: <https://doi.org/10.1007/s00015-010-0043-z>
- Kamleitner, S., Ivy-Ochs, S., Manatschal, L., Akçar, N., Christl, M., Vockenhuber, C., et al. (2023) Last Glacial Maximum glacier fluctuations on the northern Alpine foreland: geomorphological and chronological reconstructions from the Rhine and Reuss glacier systems. *Geomorphology*, 423, 108548. Available from: <https://doi.org/10.1016/j.geomorph.2022.108548>
- Keller, O. (1981) Zur Glazialmorphologie der Region St. Gallen: Die eiszeitliche Ausgestaltung der Landschaft. In: Schmid, R. & Keller, O. (Eds.) *Berichte Über Die Tätigkeit Der St. Gallischen Naturwissenschaftlichen Gesellschaft Während Der Vereinsjahre 1973 Bis 1981*. 81. Band. Rorschach: Druckerei Lehner, pp. 29–72.
- Keller, O. (2021) The landscape of the Rhine Glacier in the Lake Constance area. In: Reynard, E. (Ed.) *Landscapes and landforms of Switzerland*, World Geomorphological Landscapes. Cham: Springer, pp. 289–304. Available from: [https://doi.org/10.1007/978-3-030-43203-4\\_20](https://doi.org/10.1007/978-3-030-43203-4_20)

- Keller, O. & Krays, E. (1980) Die letzte Vorlandvereisung in der Nordostschweiz und im Bodensee-Raum (Stadialer Komplex Würm-Stein am Rhein). *Eclogae Geologicae Helveticae*, 73, 823–838.
- Keller, O. & Krays, E. (2000) Die Hydrographie des Bodenseeraums in Vergangenheit und Gegenwart. *Berichte der St. Gallischen Naturwissenschaftlichen Gesellschaft*, 89, 39–56.
- Keller, O. & Krays, E. (2005) Der Rhein-Linth-Gletscher im letzten Hochglazial. 1. Teil: Einleitung; Aufbau und Abschmelzen des Rhein-Linth-Gletschers im Oberen Würm. *Vierteljahrsschrift der Naturforschenden Gesellschaft in Zürich*, 150, 19–32.
- Kleman, J. & Borgström, I. (1996) Reconstruction of palaeo-ice sheets: the use of geomorphological data. *Earth Surface Processes and Landforms*, 21(10), 893–909. Available from: [https://doi.org/10.1002/\(SICI\)1096-9837\(199610\)21:10<893::AID-ESP620>3.0.CO;2-U](https://doi.org/10.1002/(SICI)1096-9837(199610)21:10<893::AID-ESP620>3.0.CO;2-U)
- Kleman, J., Hättetstrand, C., Stroeven, A.P., Jansson, K.N., De Angelis, H. & Borgström, I. (2007) Reconstruction of palaeo-ice sheets—inversion of their glacial geomorphological record. In: Knight, P.G. (Ed.) *Glacier science and environmental change*. Oxford: Blackwell Publishing, pp. 192–198. Available from: <https://doi.org/10.1002/9780470750636.CH38>
- Knight, J. & McCabe, A.M. (1997) Identification and significance of ice-flow-transverse subglacial ridges (Rogen moraines) in northern central Ireland. *Journal of Quaternary Science*, 12, 519–524. Available from: [https://doi.org/10.1002/\(SICI\)1099-1417\(199711/12\)12:6<519::AID-JQS313>3.0.CO;2-Q](https://doi.org/10.1002/(SICI)1099-1417(199711/12)12:6<519::AID-JQS313>3.0.CO;2-Q)
- Krüger, J. & Thomsen, H.H. (1984) Morphology, stratigraphy, and genesis of small drumlins in front of the glacier Mýrdalsjökull, South Iceland. *Journal of Glaciology*, 30(104), 94–105. Available from: <https://doi.org/10.3189/S002214300008534>
- Lindgren, A., Hugelius, G., Kuhry, P., Christensen, T.R. & Vandenberghe, J. (2016) GIS-based maps and area estimates of Northern Hemisphere permafrost extent during the Last Glacial Maximum. *Permafrost and Periglacial Processes*, 27(1), 6–16. Available from: <https://doi.org/10.1002/ppp.1851>
- Ludwig, A. (1930) *Geologischer Atlas der Schweiz 1:25 000 Blätter 218 Flawil 219 Herisau 220 Brunnadern 221 Schwellbrunn*. Bern: A. Francke A.G.
- McMartin, I., Godbout, P.M., Campbell, J.E., Tremblay, T. & Behnia, P. (2021) A new map of glacial features and glacial landforms in central mainland Nunavut, Canada. *Boreas*, 50(1), 51–75. Available from: <https://doi.org/10.1111/BOR.12479>
- Menzies, J. (1979) A review of the literature on the formation and location of drumlins. *Earth-Science Reviews*, 14(4), 315–359. Available from: [https://doi.org/10.1016/0012-8252\(79\)90093-X](https://doi.org/10.1016/0012-8252(79)90093-X)
- Menzies, J. & Habbe, K.A. (1992) A cryogenic wedge within gravels, north of Kempten, Bavaria, F.R.G. *Zeitschrift für Geomorphologie*, 36(3), 365–374. Available from: <https://doi.org/10.1127/zfg/36/1992/365>
- Menzies, J. & Maltman, A.J. (1992) Microstructures in diamictons—evidence of subglacial bed conditions. *Geomorphology*, 6(1), 27–40. Available from: [https://doi.org/10.1016/0169-555X\(92\)90045-P](https://doi.org/10.1016/0169-555X(92)90045-P)
- Möller, P. & Dowling, T.P.F. (2018) Equifinality in glacial geomorphology: instability theory examined via ribbed moraine and drumlins in Sweden. *GFF*, 140(2), 106–135. Available from: <https://doi.org/10.1080/11035897.2018.1441903>
- Moore, H.D. (1989) Drumlin formation: a time transgressive model. *Boreas*, 18(2), 99–107. Available from: <https://doi.org/10.1111/j.1502-3885.1989.tb00379.x>
- Napieralski, J., Harbor, J. & Li, Y. (2007) Glacial geomorphology and geographic information systems. *Earth-Science Reviews*, 85(1–2), 1–22. Available from: <https://doi.org/10.1016/J.EARSCIREV.2007.06.003>
- Napieralski, J. & Nalepa, N. (2010) The application of control charts to determine the effect of grid cell size on landform morphometry. *Computational Geosciences*, 36(2), 222–230. Available from: <https://doi.org/10.1016/j.cageo.2009.06.003>
- Ng, F.S.L. & Hughes, A.L.C. (2019) Reconstructing ice-flow fields from streamlined subglacial bedforms: a kriging approach. *Earth Surface Processes and Landforms*, 44(4), 861–876. Available from: <https://doi.org/10.1002/esp.4538>
- Patterson, C.J. & Hooke, R.L. (1995) Physical environment of drumlin formation. *Journal of Glaciology*, 41(137), 30–38. Available from: <https://doi.org/10.3189/S002214300017731>
- Pavoni, N., Jäckli, H. & Schindler, C. (1992) *Blatt 1091 Zürich*.—*Geol. Atlas Schweiz 1:25 000, Karte 90*. Wabern: Bundesamt für Landestopografie swisstopo.
- Penck, A. & Brückner, E. (1909) *Die Alpen im Eiszeitalter*. Leipzig: Chr. Herm. Tauchnitz.
- Pietsch, J. & Jordan, P. (2014) *Arbeitsbericht NAB 14-02. Digitales Höhenmodell Basis Quartär der Nordschweiz—Version 2014 und ausgewählte Auswertungen*. Wettingen: Nagra.
- Prest, V.K., Grant, D.R. & Rampton, V.N. (1968) *Glacial map of Canada, map 1253A*. Ottawa: Canada Department of Energy, Mines and Resources.
- Preusser, F., Blei, A., Graf, H. & Schlüchter, C. (2007) Luminescence dating of Würmian (Weichselian) proglacial sediments from Switzerland: methodological aspects and stratigraphical conclusions. *Boreas*, 36(2), 130–142. Available from: <https://doi.org/10.1111/j.1502-3885.2007.tb01187.x>
- Preusser, F., Graf, H.R., Keller, O., Krays, E. & Schlüchter, C. (2011) Quaternary glaciation history of northern Switzerland. *E&G Quaternary Science Journal*, 60(2/3), 282–305. Available from: <https://doi.org/10.3285/eg.60.2-3.06>
- Preusser, F., Reitner, J.M. & Schlüchter, C. (2010) Distribution, geometry, age and origin of overdeepened valleys and basins in the Alps and their foreland. *Swiss Journal of Geosciences*, 103(3), 407–426. Available from: <https://doi.org/10.1007/s00015-010-0044-y>
- Punkari, M. (1980) The ice lobes of the Scandinavian ice sheet during the deglaciation in Finland. *Boreas*, 9(4), 307–310. Available from: <https://doi.org/10.1111/j.1502-3885.1980.tb00710.x>
- Punkari, M. (1997) Glacial and glaciofluvial deposits in the interlobate areas of the Scandinavian ice sheet. *Quaternary Science Reviews*, 16(7), 741–753. Available from: [https://doi.org/10.1016/S0277-3791\(97\)00020-6](https://doi.org/10.1016/S0277-3791(97)00020-6)
- Putkinen, N., Eyles, N., Putkinen, S., Ojala, A.E.K., Palmu, J.P., Sarala, P., et al. (2017) High-resolution LiDAR mapping of glacial landforms and ice stream lobes in Finland. *Bulletin of the Geological Society of Finland*, 89(2), 64–81. Available from: <https://doi.org/10.17741/bgsf/89.2.001>
- Regierungspräsidium Freiburg Landesamt für Geologie, Rohstoffe und Bergbau, (2013) *Geologische Karte 1:50 000, Geodaten der Integrierten Geowissenschaftlichen Landesaufnahme (GeoLa)*. Freiburg: Regierungspräsidium Freiburg, Landesamt für Geologie, Rohstoffe und Bergbau.
- Rey, R., Wildberger, A., Frank, S. & Freimoser, M. (2011) *Blatt 1072 Winterthur*.—*Geol. Atlas Schweiz 1:25 000, Karte 140*. Wabern: Bundesamt für Landestopografie swisstopo.
- Salcher, B.C., Hinsch, R. & Wagreich, M. (2010) High-resolution mapping of glacial landforms in the North Alpine Foreland, Austria. *Geomorphology*, 122(3–4), 283–293. Available from: <https://doi.org/10.1016/j.geomorph.2009.09.037>
- Saxer, F. (1965) *Geologischer Atlas der Schweiz 1:25 000 Blatt: 1075 Rorschach*. Bern: Kümmerly & Frey AG.
- Schaller, S., Böttcher, M.E., Buechi, M.W., Epp, L.S., Fabbri, S.C., Gribenski, N., et al. (2022) Postglacial evolution of Lake Constance: sedimentological and geochemical evidence from a deep-basin sediment core. *Swiss Journal of Geosciences*, 115(1), 7. Available from: <https://doi.org/10.1186/s00015-022-00412-1>
- Schindler, C., Röthlisberger, H. & Gyger, M. (1978) Glaziale Stauchungen in den Niederterrassen-Schottern des Aadorfer Feldes und ihre Deutung. *Eclogae Geologicae Helveticae*, 71, 159–174.
- Schlunegger, F. & Mosar, J. (2011) The last erosional stage of the Molasse Basin and the Alps. *International Journal of Earth Sciences*, 100(5), 1147–1162. Available from: <https://doi.org/10.1007/S00531-010-0607-1/FIGURES/6>
- Schmidle, W. (1914) *Die diluviale Geologie der Bodenseegegend, Die Rheinlande in naturwissenschaftlichen und geographischen Einzeldarstellungen Nr. 8*. Braunschweig: Westermann.
- Schmidle, W. (1916) *Geologische Spezialkarte des Grossherzogtums Baden, 1: 25 000. Blatt 162 Konstanz, mit Erläuterungen [unveränd. Nachdruck*

- als Geologische Karte von Baden-Württemberg, 1:25 000. Blatt 8321 Konstanz-Ost]. Stuttgart: Geologisches Landesamt Baden-Württemberg.
- Schmidt, A. & Münst, M. (1979) Erläuterungen zu Blatt 8323 Tettang. In: *Geologische Karte Baden-Württemberg 1:25 000*. Stuttgart: Geologisches Landesamt Baden-Württemberg.
- Schmidt, M. & Bräuhäuser, M. (1985) *Erläuterungen zu Blatt 8324 Wangen im Allgäu–West, Geologische Karte von Baden-Württemberg 1:25 000 Bl. 8324*. Freiburg im Breisgau: Geologisches Landesamt Baden-Württemberg.
- Schnellmann, M., Fischer, U., Heuberger, S. & Kober, F. (2014) *Arbeitsbericht NAB 14-25. Erosion und Landschaftsentwicklung Nordschweiz Zusammenfassung der Grundlagen im Hinblick auf die Beurteilung der Langzeitstabilität eines geologischen Tiefenlagers (SGT Etappe 2)*. Wettingen: Nagra.
- Schreiner, A. (1968) Eiszeitliche Rinnen und Becken und deren Füllung im Hegau und westlichen Bodenseegebiet. *Jahreshefte des Geologischen Landesamts Baden-Württemberg*, 10, 79–104.
- Schreiner, A. (1976) Drumlins oder Schmelzwasserkuppen in der Jungmoräne bei Tettang (Oberschwaben, Baden-Württemberg). *Jahreshefte des Geologischen Landesamts Baden-Württemberg*, 18, 113–120.
- Schreiner, A. (1979) Zur Entstehung des Bodenseebeckens. *E&G Quaternary Science Journal*, 29(1), 71–76. Available from: <https://doi.org/10.3285/eg.29.1.07>
- Schreiner, A. (1992a) *Einführung in die Quartärgeologie*. Stuttgart: E. Schweizerbart'sche.
- Schreiner, A. (1992b) *Erläuterungen zu Blatt Hegau und westlicher Bodensee–3. Aufl., Geologische Karte 1:50 000 von Baden-Württemberg*. Freiburg im Breisgau, Stuttgart: Geologisches Landesamt Baden-Württemberg.
- Schuster, R., Pestal, G. & Reitner, J.M. (2006) *Erläuterungen zu Blatt 182 Spittal an der Drau*. Wien: Geologische Bundesanstalt.
- Seguinot, J., Ivy-Ochs, S., Jouvet, G., Huss, M., Funk, M. & Preusser, F. (2018) Modelling last glacial cycle ice dynamics in the Alps. *The Cryosphere*, 12(10), 3265–3285. Available from: <https://doi.org/10.5194/tc-12-3265-2018>
- Shaw, J. (2002) The meltwater hypothesis for subglacial bedforms. *Quaternary International*, 90(1), 5–22. Available from: [https://doi.org/10.1016/S1040-6182\(01\)00089-1](https://doi.org/10.1016/S1040-6182(01)00089-1)
- Shaw, J., Sharpe, D. & Harris, J. (2010) A flowline map of glaciated Canada based on remote sensing data. *Canadian Journal of Earth Sciences*, 47(1), 89–101. Available from: [https://doi.org/10.1139/E09-068/SUPPL\\_FILE/E09-068MAP.GIF](https://doi.org/10.1139/E09-068/SUPPL_FILE/E09-068MAP.GIF)
- Smith, M.J. & Clark, C.D. (2005) Methods for the visualization of digital elevation models for landform mapping. *Earth Surface Processes and Landforms*, 30(7), 885–900. Available from: <https://doi.org/10.1002/esp.1210>
- Smith, M.J., Rose, J. & Booth, S. (2006) Geomorphological mapping of glacial landforms from remotely sensed data: an evaluation of the principal data sources and an assessment of their quality. *Geomorphology*, 76(1-2), 148–165. Available from: <https://doi.org/10.1016/j.geomorph.2005.11.001>
- Sookhan, S., Eyles, N. & Arbelaez-Moreno, L. (2018) Converging ice streams: a new paradigm for reconstructions of the Laurentide Ice Sheet in southern Ontario and deposition of the Oak Ridges Moraine. *Canadian Journal of Earth Sciences*, 55(4), 373–396. Available from: <https://doi.org/10.1139/cjes-2017-0180>
- Spagnolo, M., Clark, C.D., Ely, J.C., Stokes, C.R., Anderson, J.B., Andreassen, K., et al. (2014) Size, shape and spatial arrangement of mega-scale glacial lineations from a large and diverse dataset. *Earth Surface Processes and Landforms*, 39(11), 1432–1448. Available from: <https://doi.org/10.1002/esp.3532>
- Spagnolo, M., Clark, C.D., Hughes, A.L.C. & Dunlop, P. (2011) The topography of drumlins; assessing their long profile shape. *Earth Surface Processes and Landforms*, 36(6), 790–804. Available from: <https://doi.org/10.1002/esp.2107>
- Spagnolo, M., Clark, C.D., Hughes, A.L.C., Dunlop, P. & Stokes, C.R. (2010) The planar shape of drumlins. *Sedimentary Geology*, 232(3-4), 119–129. Available from: <https://doi.org/10.1016/j.sedgeo.2010.01.008>
- Stokes, C.R. (2018) Geomorphology under ice streams: moving from form to process. *Earth Surface Processes and Landforms*, 43(1), 85–123. Available from: <https://doi.org/10.1002/esp.4259>
- Stokes, C.R. & Clark, C.D. (2001) Palaeo-ice streams. *Quaternary Science Reviews*, 20(13), 1437–1457. Available from: [https://doi.org/10.1016/S0277-3791\(01\)00003-8](https://doi.org/10.1016/S0277-3791(01)00003-8)
- Stokes, C.R. & Clark, C.D. (2002) Are long subglacial bedforms indicative of fast ice flow? *Boreas*, 31(3), 239–249. Available from: <https://doi.org/10.1111/J.1502-3885.2002.TB01070.X>
- Stokes, C.R., Clark, C.D., Lian, O.B. & Tulaczyk, S. (2007) Ice stream sticky spots: a review of their identification and influence beneath contemporary and palaeo-ice streams. *Earth-Science Reviews*, 81(3-4), 217–249. Available from: <https://doi.org/10.1016/J.EARSCIREV.2007.01.002>
- Stokes, C.R., Fowler, A.C., Clark, C.D., Hindmarsh, R.C.A. & Spagnolo, M. (2013) The instability theory of drumlin formation and its explanation of their varied composition and internal structure. *Quaternary Science Reviews*, 62, 77–96. Available from: <https://doi.org/10.1016/j.quascirev.2012.11.011>
- Stokes, C.R., Lian, O.B., Tulaczyk, S. & Clark, C.D. (2008) Superimposition of ribbed moraines on a palaeo-ice-stream bed: implications for ice stream dynamics and shutdown. *Earth Surface Processes and Landforms*, 33(4), 593–609. Available from: <https://doi.org/10.1002/ESP.1671>
- Stokes, C.R., Spagnolo, M. & Clark, C.D. (2011) The composition and internal structure of drumlins: complexity, commonality, and implications for a unifying theory of their formation. *Earth-Science Reviews*, 107(3-4), 398–422. Available from: <https://doi.org/10.1016/j.earscirev.2011.05.001>
- Stokes, C.R., Spagnolo, M., Clark, C.D., Ó Cofaigh, C., Lian, O.B. & Dunstone, R.B. (2013) Formation of mega-scale glacial lineations on the Dubawnt Lake Ice Stream bed: 1. Size, shape and spacing from a large remote sensing dataset. *Quaternary Science Reviews*, 77, 190–209. Available from: <https://doi.org/10.1016/j.quascirev.2013.06.003>
- Strasky, S., Morard, A. & Möri, A. (2016) Harmonising the lithostratigraphic nomenclature: towards a uniform geological dataset of Switzerland. *Swiss Journal of Geosciences*, 109(2), 123–136. Available from: <https://doi.org/10.1007/s00015-016-0221-8>
- Sutinen, R., Jakonen, M., Piekari, M., Haavikko, P., Närhi, P. & Middleton, M. (2010) Electrical-sedimentary anisotropy of Rogen moraine, Lake Rogen area, Sweden. *Sedimentary Geology*, 232(3-4), 181–189. Available from: <https://doi.org/10.1016/j.sedgeo.2010.07.007>
- Swisstopo. (2018a) Felsoberflächenmodell (TopFels25).
- Swisstopo. (2018b) SwissALTI<sup>3D</sup>. Das hoch aufgelöste Terrainmodell der Schweiz. Produktinformation 17.
- Szuman, I., Kalita, J.Z., Ewertowski, M.W., Clark, C.D. & Livingstone, S.J. (2021) Dynamics of the last Scandinavian Ice Sheet's southernmost sector revealed by the pattern of ice streams. *Boreas*, 50(3), 764–780. Available from: <https://doi.org/10.1111/bor.12512>
- van der Meer, J.J.M. (1982) A recent drumlin with fluted surface in the Swiss Alps. In: Evenson, E.B., Schlüchter, C. & Rabassa, J. (Eds.) *Tills and related deposits*. Rotterdam: A. A. Balkema, pp. 105–109.
- van Husen, D. (1977) *Zur Fazies und Stratigraphie der jungpleistozänen Ablagerungen im Trauntal*. Wien: Geologische Bundesanstalt.
- van Husen, D. (1987) *Die Ostalpen und ihr Vorland in der letzten Eiszeit (Würm)*. Wien: Geologische Bundesanstalt.
- Vandenberghe, J., French, H.M., Gorbunov, A., Marchenko, S., Velichko, A.A., Jin, H., et al. (2014) The Last Permafrost Maximum (LPM) map of the Northern Hemisphere: permafrost extent and mean annual air temperatures, 25–17 ka BP. *Boreas*, 43(3), 652–666. Available from: <https://doi.org/10.1111/bor.12070>
- Wagner, K. (2017) Geographic information systems and glacial environments. In: Menzies, J. & van der Meer, J.J.M. (Eds.) *Past glacial environments*. Amsterdam: Elsevier, pp. 503–536. Available from: <https://doi.org/10.1016/B978-0-08-100524-8.00015-4>

- Weinberger, L. (1952) Ein Rinnensystem im Gebiete des Salzach-Gletschers. *Zeitschrift für Gletscherkunde und Glazialgeologie*, 2, 58–71.
- Wessels, M., Anselmetti, F., Artuso, R., Baran, R., Daut, G., Gaide, S., et al. (2015) Bathymetry of Lake Constance—a high-resolution survey in a large, deep lake. *ZfV—Zeitschrift für Geodäsie, Geoinformation und Landmanagement*, 140, 203–210. Available from: <https://doi.org/10.12902/zfv-0079-2015>
- Wyssling, G. (2007) *Blatt 1092 Uster*.—*Geol. Atlas Schweiz 1:25 000, Karte 128*. Wabern: Bundesamt für Landestopografie swisstopo.
- Zaugg, A. (2007) *Blatt 1055 Romanshorn*.—*Geol. Atlas Schweiz 1:25 000, Karte 125*. Wabern: Bundesamt für Landestopografie swisstopo.
- Zaugg, A. & Geyer, M. (2008) *Blatt 1033/1034 Steckborn-Kreuzlingen*.—*Geol. Atlas Schweiz 1:25 000, Karte 112*. Wabern: Bundesamt für Landestopografie swisstopo.
- Zaugg, A., Geyer, M., Rahn, M., Wessels, M., Schlichtherle, H., Hasenfratz, A., et al. (2008) *Erläuterungen zum Geologischen Atlas der Schweiz 1:25 000, Blatt 1033 Steckborn (Südteil) mit SW-Anteil von*

1034 Kreuzlingen. Wabern: Bundesamt für Landestopografie swisstopo.

## SUPPORTING INFORMATION

Additional supporting information can be found online in the Supporting Information section at the end of this article.

**How to cite this article:** Kamleitner, S., Ivy-Ochs, S., Salcher, B. & Reitner, J.M. (2024) Reconstructing basal ice flow patterns of the Last Glacial Maximum Rhine glacier (northern Alpine foreland) based on streamlined subglacial landforms. *Earth Surface Processes and Landforms*, 49(2), 746–769. Available from: <https://doi.org/10.1002/esp.5733>